Small molecules for modulating protein driven liquid-liquid phase separation in treating neurodegenerative disease

Richard J. Wheeler[1,2], Hyun O. Lee[1,3], Ina Poser[1], Arun Pal[4,5], Thom Doeleman[4,5], Satoshi Kishigami[6], Sukhleen Kour[7,8,9], Eric Nathaniel Anderson[7,8,9], Lara Marrone[5,10] , Anastasia C. Murthy[11], Marcus Jahnel[1], Xaiojie Zhang[1], Edgar Boczek[1], Anatol Fritsch[1], Nicolas L. Fawzi[12], Jared Sterneckert[5,10], Udai Pandey[7,8,9], Della C. David[13], Benjamin G. Davis[6], Andrew J. Baldwin[6], Andreas Hermann[13,15,16], Marc Bickle[1], Simon Alberti[1,17], Anthony A. Hyman[1,17]*
* To whom correspondence should be addressed: hyman@mpi-cbg.de

[1] Max Planck Institute of Molecular Cell Biology and Genetics, Pfotenhauerstraße 108, Dresden, Germany
[2] Current address: Peter Medawar Building for Pathogen Research, Nuffield Department of Medicine, University of Oxford, South Parks Road, Oxford, UK
[3] Current address: Biochemistry, University of Toronto, MaRS, West Tower, Suite 1501 661 University Avenue, Toronto, Ontario, Canada.
[4] Department of Neurology, Technische Universität Dresden, Dresden, Germany
[5] Center for Regenerative Therapies (CRT), Dresden, Germany
[6] Department of Chemistry, University of Oxford, South Parks Road, Oxford, UK
[7] Division of Child Neurology, Department of Pediatrics, Children's Hospital of Pittsburgh, University of Pittsburgh Medical Center, Pittsburgh, PA, USA
[8] Department of Human Genetics, University of Pittsburgh Graduate School of Public Health, Pittsburgh, PA, USA
[9] Department of Neurology, University of Pittsburgh School of Medicine, Pittsburgh, PA, USA
[10] Centre for Regenerative Therapies, Technische Universität Dresden, Dresden, Germany
[11] Graduate Program in Molecular Biology, Cell Biology and Biochemistry, Brown University, Providence, RI, USA.
[12] Department of Molecular Pharmacology, Physiology, and Biotechnology, Brown University, Providence, RI, USA
[13] German Centre for Neurodegenerative Diseases, Otfried-Müller-Straße 23, Tübingen, Germany
[14] Translational Neurodegeneration Section “Albrecht-Kossel”, Department of Neurology, University Medical Center Rostock, University of Rostock, Rostock, Germany
[15] Center for Transdisciplinary Neurosciences Rostock (CTNR), University Medical Center Rostock, University of Rostock, 18147 Rostock, Germany
[16] German Center for Neurodegenerative Diseases (DZNE) Rostock/Greifswald, 18147 Rostock, Germany
[17] Dewpoint Therapeutics, Cambridge, MA 02139, USA
[18] Current address: Dewpoint Therapeutics, Cambridge, MA 02139, USA

Abstract

Amyotrophic lateral sclerosis (ALS) is a neurodegenerative disease with few avenues for treatment. Many proteins implicated in ALS associate with stress granules, which are examples of liquid-like compartments formed by phase separation. Aberrant phase transition of stress granules has been implicated in disease, suggesting that modulation of phase transitions could be a possible therapeutic route. Here, we combine cell-based and protein-based screens to show that lipoamide, and its related compound lipoic acid, reduce the propensity of stress granule proteins to aggregate *in vitro.* More significantly, they also prevented aggregation of proteins over the life time of *Caenorhabditis elegans*. Observations that they prevent dieback of ALS patient-derived (FUS mutant) motor neuron axons in culture and recover motor defects in *Drosophila melanogaster* expressing FUS mutants suggest plausibility as effective therapeutics. Our results suggest that altering phase behaviour of stress granule proteins in the cytoplasm could be a novel route to treat ALS.

Introduction

ALS is a fatal neurodegenerative disease with poor prognosis and few options for therapy[1]. Most forms of ALS are sporadic but around 10% are monogenic disorders[2]. Currently only two FDA approved drugs are available, riluzole and edaravone, however both only slow disease progression by a few months[3,4]. The mechanisms of riluzole and edaravone are not well understood and most likely do not directly target the underlying pathomechanism[3]. New approaches are therefore needed.

The precise mechanism of ALS pathogenesis is not known. Recent work has focused on familial ALS-associated mutations that are frequently found in RNA-binding proteins (RBPs) such as FUS (**fu**sed in **s**arcoma) and TDP-43 (**T**AR **D**NA-binding **p**rotein **43**)[5,6] which have characteristic low complexity domains (LCDs) and are part of a broader class of intrinsically disordered proteins. Mutated TDP-43 and FUS often mislocalise to the cytoplasm where they promote stress granule formation and sometimes form cytoplasmic aggregates associated with disease[7–9].

Stress granules are inducible RNP granules that form in the cytoplasm of eukaryotic cells upon stress. They contain non-translated mRNAs and are thought to be involved in the shut-down of translation during stress[10]. Stress granules have attracted considerable attention in recent years because of their relationship to human disease [6,11,12]. Evidence is accumulating that aberrant forms of stress granules can result from liquid-to-solid transitions, and that these aberrant forms of stress granules underlie disease [7,13–15]. This suggests in turn that dissolving stress granules and/or aggregated stress granule proteins could help ameliorate disease.

Stress granules are liquid-like membraneless compartments that have been proposed to form by liquid-liquid phase separation[7,16–18]. In principle, it might be possible to target the physical chemistry driving stress granule formation to modulate them[19]. Indeed, there are a few compounds known to disrupt stress granule phase separation: 1,6-hexanediol[20–22] and similar alcohols[23,24]. However, these compounds suffer from two problems: First, they require extremely high concentrations (1-10% v/v) and are toxic[23,25]. Second, the effects of these alcohols are not specific to stress granules and affect other membraneless liquid compartments that are also liquid-like, such as the nucleolus. This suggests that identifying compounds that more specifically modulate phase separation of certain compartments could be important in therapeutic intervention.

We screened a small library of medicinal compounds (1600 drugs and compounds with known biological targets) to discover those that affect stress granule formation, using FUS as a well-characterised stress granule component target. This identified lipoamide and lipoic acid, which are

non-toxic and relieved the effects of ALS-associated FUS mutations *in vivo* in different systems, namely, stress granule protein aggregation in worms (*Caenorhabditis elegans*), motor dysfunction in a *Drosophila melanogaster* model of familial ALS, and the motor neuron die-back *in vitro* in patient-derived iPSCs carrying a FUS mutant associated with familial ALS. Together these suggest a plausible novel route to ALS therapeutics.

Results

Multi-parameter cellular image analysis screening identified lipoamide as a molecule that reduces stress granule formation

We developed a cell-based screen using a HeLa cell line that stably expresses a GFP-FUS fusion protein at near-endogenous levels[7]. While not required for stress granule formation, FUS is a well-characterised protein with a domain structure typical of stress granule proteins[26]. In the absence of cellular stress, FUS-GFP primarily localizes to the nucleus, where it is partially excluded from the nucleolus (Figure 1A). It also localises to small puncta called paraspeckles – these nuclear condensates are implicated in retaining RNA in the nucleus for rapid stress response[27]. In stressed cells, FUS is partly exported to the cytoplasm where, in combination with other proteins and mRNA, it phase separates to concentrate in liquid-like stress granules surrounded by cytoplasm consequently depleted in FUS[7,28] (Figure 1A). In our screen we pre-treated cells with 10 µM compound from a compound library for 1 h, then stressed the cells with 1 mM potassium arsenate (still in the presence of compound) (Figure 1B) and monitored FUS localization to stress granules. Arsenate disrupts antioxidant responses by reacting with thiol groups, blocks the tricarboxylic acid (TCA) cycle by reacting with the thiols in vital lipoyl moieties and causes general oxidative damage[29,30].

We used multi-parameter image analysis to determine the effect of compounds on FUS localisation in stressed cells – an image-based approach was necessary to identify compounds affecting stress granule formation rather than using a biochemical readout. Compounds were ranked by strength of effect on FUS localisation (Figure 1C) with cytoplasmic puncta number, nuclear puncta number and nuclear/cytoplasm partition typically showing the largest changes. Two compounds in the library were expected to give a reduction of stress granules. These were the polysome stabilising compound emetine[31], which prevents release of mRNA, and the heavy metal chelating compound dimercaprol, which chelates arsenic and has beneficial effects in animals on arsenate toxicity[32] (Figure 1C). Notably edaravone, thought to be an antioxidant[33] and used as an ALS therapeutic in Japan and the USA[34], had no effect on FUS localisation in arsenate-stressed cells. Compound classes which tended

to have a large effect on FUS localisation, typically reducing stress granule number, included cardiac glycosides, heterotri- and tetracyclic compounds (anthraquinones and acridines), surfactants and benzimidazoles.

The compounds with the strongest effects on intracellular FUS localisation were then tested for direct interaction with FUS condensate droplets formed under low salt conditions *in vitro*, carried out in the presence of 1 mM DTT to mimic the reducing intracellular environment. In a moderate-throughput screen we determined the effect of the 47 strongest in cell hits on the number of FUS condensate droplets formed or the ratio of FUS GFP signal inside the droplets to outside (partition into the droplets) (Figure 2A). Of these 47 compounds 7 significantly affected FUS *in vitro* (Figure 2B) and fell into just three compound classes: heterotri- and tetracyclic compounds, surfactants and lipoamide (Figure 2C,D). In this non-equilibrium snapshot, the heterotri- and tetracyclic compounds tended to reduce condensate formation in a dose-dependent manner and the resulting droplets were smaller. In contrast, surfactants and lipoamide tended to increase condensate droplet number, partition into droplets and the droplets were larger (Figure 2B,D). Surfactants are not plausible therapeutics as they will permeabalise cell membranes, and were present in the library due to their use as topical antiseptics. Both lipoamide and its closely related compound lipoic acid are non-toxic and lipoic acid has well-characterised pharmacokinetics: 1,600 mg orally gives plasma concentrations of 8 to 30 µM in humans[35,36] and has a long history of use in diabetic neuropathy therapy at doses around 600 mg/day[37]. Through the remainder of this work we therefore selected the lipoamide class as of primary interest with some comparison to mitoxantrone as an example of a heterotricyclic compound.

Lipoamide action in cells is non-enzymatic and non-antioxidant

The stressor, arsenate, will react with the thiol groups of lipoamide. Therefore, to exclude the possibility that lipoamide is acting only by removing the stressor we tested whether it can prevent stress granule formation triggered by other non-arsenate stresses: Mitochondrial electron transport chain inhibition (rotenone), heat stress (42°C), hyperosmotic stress (sorbitol, a non-metabolisable sugar), glycolysis inhibition (6-deoxyglucose in the absence of glucose) or serum starvation. 10 µM lipoamide reduced stress granule formation in HeLa cells with mitochondrial, hyperosmotic or arsenate stress but not heat or glycolysis stress (Figure 3A). Lipoamide is therefore not only reacting with arsenate but reduces stress granule formation under several cellular stresses.

Lipoic acid is a compound similar to lipoamide which plays a part in normal cellular metabolism and was a weaker hit in the cell screen (Figure 1C). Of the two lipoic acid stereoisomers R-(+)-lipoic acid naturally occurs in cells and is synthesised in the mitochondrion while S-(−)-lipoic acid is not.

However R-(+)-lipoic acid is present at very low free concentrations in the cell – it is biosynthesised, and therefore normally found, covalently bonded to proteins as a lipoyl moiety attached to the sidechain of lysyl residues as a lipoamide. These compounds are cyclic disulfides and the corresponding reduced dithiol forms of the lipoyl moiety are used by several mitochondrial metabolic enzymes, including dihydrolipoyl transacetylase feeding into the TCA cycle and dihydrolipoamide succinyltransferase in the TCA cycle. The R-(+) isomer is reduced from the cyclic disulphide to the dithol state in cells by dihydrolipoamide dehydrogenase[38], however its natural substrate is the lipoyl moiety rather than free lipoic acid. We determined whether 10 µM R-(+), S-(−) or racemic (±, a mix of both stereoisomers) lipoic acid also reduced stress granule formation in HeLa cells. This showed both lipoic acid isomers also reduce stress granule formation under mitochondrial, hyperosmotic or arsenate stress, as seen for lipoamide (Figure 3A).

Next, we analysed the dose dependent activity of lipoamide, lipoic acid and related compounds. Lipoamide gave a reduction of stress granule number with an EC_{50} around 20 µM in both HeLa cells and induced pluripotent stem cells (iPS) cells following 1 h of 1 mM arsenate stress (Figure 3B,C). Lipoamide also caused FUS to return to the nucleus, as shown by a dose-dependent increase in nuclear/cytoplasm partitioning of FUS (Figure 3B,C). We noted that the heterotri- and tetracyclic compounds, including mitoxantrone, had the inverse effect on nuclear/cytoplasm partition (Figure S1). Return of FUS to the nucleus is likely beneficial, mimicking the unstressed cell state[39,40], indicating lipoamide is a more promising candidate.

In HeLa cells (±)-dihydrolipoic acid and (±), R-(+) and S-(−)-lipoic acid had a similar EC_{50}, a little higher than (±)-lipoamide (Figure 3D,E). Valeric acid and 1,3-propanedithiol had no effect up to 100 µM (Figure 3D,E). In the cellular reducing environment it is likely that the lipoamide/lipoic acid cyclic disulfide is reduced to a dithol and the similar EC_{50} of (±)-dihydrolipoic acid and (±)-lipoic acid is consistent with this. Lipoic acid has been proposed to be an antioxidant[41], although evidence for direct action as an antioxidant is disputed[42]. Cellular antioxidant effects involving an enzymatic redox cycle will involve dihydrolipoamide dehydrogenase, which is more active for the naturally occurring R-(+) isomer although normally reduces lipoyl moieties[38,43]. However S-(−)-lipoic acid had very similar activity to R-(+)-lipoic acid (Figure 3C,D). We also note that classic antioxidants such as menadione (pro-vitamin K) and edaravone did not reduce stress granule number in the primary HeLa cell screen. Any enzymatic role in the activity of lipoic acid as a coenzyme/addition to an apoenzyme requires a lipoate-protein ligase[44], likely specific to R-(+)-lipoic acid. The similar activity of S-(−) and R-(+)-lipoic acid and absence of a clear human lipoate-protein ligase indicates this is unlikely (Figure 3C,D). Together, this indicates a non-antioxidant and non-metabolic mechanism of action; perhaps a stress

signaling mechanism or a direct effect on the physical chemistry of phase separated stress granule proteins.

Lipoamide/lipoic acid dissolves stress granules

To gain insight into the breadth of action of lipoamide and lipoic acid, we comprehensively characterised their action in HeLa cells. We first determined that these compounds can lead to dissolution of existing stress granules by showing that addition of fresh medium after stress, containing 10 µM lipoamide and 1 mM arsenate, dissolved 80-90% of cytoplasmic FUS condensates within 20 minutes (Figure 4A). This response is likely too rapid to represent a transcriptional response. 1 h pre-treatment of HeLa cells with 10 µM lipoamide followed by 1 h arsenate stress without lipoamide did not prevent stress granule formation, indicating no persistent lipoamide-induced cellular adaptation to resist stress (Figure 4B).

Because several FUS-like proteins in stress granules are implicated in ALS, we anticipate a useful therapeutic would prevent other PLD-containing stress granule proteins from localising to stress granules. We used 1 mM arsenate to stress a panel of HeLa cell lines expressing GFP fusions of stress granule proteins (EWSR1, TIAL1, PABPC1, G3BP1) with either no treatment or 10 µM (±), S-(−) or R-(+)-lipoic acid or (±)-lipoamide. All proteins localised to stress granules in the absence of treatment. In the presence of lipoic acid or lipoamide the proteins either did not localise to stress granules or localised to a reduced number of stress granules (Figure 4C). All tested LCD/RBP proteins are therefore affected by lipoamide and lipoic acid treatment. As FUS is not required for stress granule formation this suggests that FUS is not the only nor necessarily a primary target of lipoamide or lipoic acid in cells. It also suggests a possible therapeutic effect on pathology arising from mutation of other stress granule proteins.

Lipoamide does not affect other cytoplasmic condensates

Stress granules are one of many important biomolecular condensates. We anticipate that a useful therapeutic would not affect all these compartments therefore we asked to what extent lipoamide was specific to affecting stress granule dissolution, using a panel of cell lines expressing GFP fusions[45]. For this analysis, we included mitoxantrone as a representative of the heterotri-/tetracyclic compound class of hits (Figure 2C). Lipoamide, under conditions that dissolve stress granules, did not affect the localization of RNA processing body (DCP1A, P-body, cytoplasmic), Cajal body (COIL, nuclear), DNA damage focus (TRP53BP1, nuclear) or nucleolus (NCB1, nuclear) proteins (Figure 5A). In contrast, mitoxantrone affected all of these compartments to some extent, while histone localisation suggested nuclear structure overall was not dramatically affected (Figure 5A). Different

non-mixing membraneless organelles likely have differing intermolecular interactions underlying their phase separation. The mode of action of lipoamide may therefore be specific to the physical chemistry driving stress granule phase separation and/or a specific signaling route. We note that stress granules normally form and dissolve rapidly in comparison to many other compartments.

In addition to testing nuclear compartments formed by other proteins we tested how the compounds influenced de novo formation of FUS-containing nuclear compartments by the recruitment of FUS to sites of DNA damage. Defective recruitment of FUS to sites of DNA damage is detrimental: FUS nuclear localization (NLS) mutations (e.g. P525L) cause altered DNA damage signalling[46] and are strongly associated of with familial ALS mutations [39]. We therefore tested whether lipoamide affect FUS GFP recruitment to sites of DNA damage in iPSCs induced by focused UV laser irradiation. We used arsenate-stressed iPSCs so that stress granules were present as an internal control for compound activity in the cytoplasm (Figure 5B). 20 µM lipoamide (which dissolved stress granules) had no significant effect on FUS GFP recruitment to sites of DNA damage. 1 µM lipoamide (which did not affect stress granules), increased recruitment of FUS GFP to sites of DNA damage, likely to be beneficial. In contrast, mitoxantrone blocked recruitment of FUS GFP to sites of DNA damage, at concentrations which were not sufficient to dissolve cytoplasmic FUS condensates.

Lipoamide affects FUS condensate behaviour *in vitro*.

We next sought to analyse the nature of direct lipoamide effects on FUS using FUS condensates *in vitro*. As for the *in vitro* screen, all assays contained excess (1 mM) of the reductant DTT which will reduce the lipoamide disulfide to free dithiols. The prior screen (Figure2, see above) had suggested drop enlargement in the presence of lipoamide. However, lipoamide at 100 µM had little effect on phase separation of FUS GFP – the resulting condensates had very similar threshold salt concentration and temperature for droplet formation (data not shown). One possibility is that lipoamide made the condensates more liquid-like. Following phase separation, average condensate droplet size increases while condensate droplet number decreases as large droplets grow at the expense of small droplets (Ostwald's ripening) and droplets fuse – both of which occur more quickly with more liquid droplets[47]. We therefore measured lipoamide effect on FUS eGFP condensate liquidity (surface tension and viscosity). Here, condensate droplets were brought together by optical tweezers and the rate of fusion and relaxation to a sphere was measured[7] (Figure 6A). Lipoamide increased the liquidity by a factor of three (Figure 6B). Together, the combined result of *in vitro* analyses suggests that the observed (Figure 2B) increases in droplet size and number arise from

faster generation of larger droplets, due to increased liquidity, followed by sedimentation of the larger droplets (see materials and methods for more details).

In vitro FUS condensates 'age' over time, first hardening then forming amyloid/prion-like fibres[7,48,49], even in the presence of 1 mM DTT as a reducing agent. This is likely represents a pathological process as it is accelerated for G156E FUS, a mutation associated with familial ALS[7]. As lipoamide/lipoic acid did not cause dissolution of FUS droplets *in vitro* we were able to examine the effect of lipoamide and lipoic acid on fibre formation and hardening, initially analysing FUS condensates formed under conditions of (dextran-induced) crowding (as previously published[7]) (Figure 6C-E) then expanded this to condensates under low salt conditions (more physiologically relevant[19,26]) (Figure 6F-H). Lipoamide and lipoic acid both delayed fibre formation of G156E FUS (Figure 6C,F) and delayed hardening of condensates, which retained a large mobile fraction of FUS (Figure 6E,H).

Finally, we analysed mechanistic detail at the sub-molecular level by using NMR of the FUS prion-like N-terminal LCD[18] to determine putative sites of lipoamide interaction. The LCD is able to phase separate to form condensates *in vitro* and the individual residues can be resolved and assigned in a ^{1}H-^{15}N heteronuclear single quantum coherence spectrum. ^{1}H-^{15}N analyses reveal a change in environment of individual residues as indicated by their corresponding chemical shifts. We compared the magnitude of chemical shift changes with and without both lipoamide or mitoxantrone (Figure S2). Whilst there were no single, clear sites of interaction of lipoamide with the FUS LCD (Figure S2B,D) mitoxantrone caused weak shifts across the LCD consistent with a weak interaction with tyrosine residues (Figure S2A,C). This suggests lipoamide does not act by direct high affinity protein binding. This leaves several possibilities: Perhaps lipoamide interacts with with the FUS LCD only when phase separated, potentially reducing viscosity, or interacts with the condensate phase boundary, perhaps increasing surface tension. Such interactions may reduce formation or expansion of aggregated forms of FUS involved in condensate hardening and reduced liquidity.

Lipoamide becomes greatly concentrated in cells

The concentration of lipoamide relative to protein required for an effect on condensate liquidity *in vitro* was higher than the EC_{50} on cells, on the order of 100 µM lipoamide with 1 µM FUS (Figure 2A,B, Figure 6). In cells, FUS concentrations are high for a protein (low µM)[50] and the cellular EC_{50} was on the order of 10 µM (Figure 3A,B). We also saw inverse effects of lipoamide on FUS-containing condensates *in vitro* (more, larger condensates) and in cells (fewer stress granules). To reconcile this difference and to understand the relevance of the effects *in vitro* in cells, we wanted to know the actual concentrations of compounds in cells. In principle, isotopic labelling allows direct monitoring

of isotopically-labelled compounds even in complex environment through appropriate spectroscopy[51]. To use this approach, ^{15}N-labelled lipoamide (Figure 7A) was synthesised. Solution state NMR experiments were then used to quantitatively detect the NH_2 protons covalently attached to ^{15}N in cells to determine lipoamide concentration from the complex mixture inside cells[51], while also revealing any chemical modification of the amide group (manifesting as chemical shift changes or spectral alterations) (Figure S3).

Uptake of ^{15}N lipoamide by cells from the medium was quantified by NMR following incubation of lipoamide at 37°C for 1 h either in the absence or presence of HeLa cells (Figure 7B). Cellular uptake was determined by calculating the difference between medium incubated with cells or without cells for combinations of either R-(+) or (±)-lipoamide and either unstressed or stressed cells (Figure 7C). For one sample, stressed cells with R-(+)-lipoamide, we confirmed that strong signal from the cell fraction was consistent with uptake of a large proportion of lipoamide (Figure 7C). Both R-(+) and ±-lipoamide measurements indicated uptake of 35±11% (n=3 and 2, respectively) of the lipoamide present in the medium. No significant difference was observed either for uptake of R-(+) compared to (±)-lipoamide or stressed compared to unstressed cells (Figure 7D). There was no evidence for metabolism or any other chemical modification of lipoamides: the NMR signal from the cell sample indicated that lipoamide was present in an unmodified form in the cells (Figure 7B).

Approximate intracellular ^{15}N lipoamide concentration can be calculated from percentage uptake, number of cells and their volume (Supplementary Methods) – these indicated an average intracellular concentration of 5.0±1.6 mM (Figure 7D), markedly higher than that attained *in vitro* under optimal conditions of H_2O with 1% v/v DMSO. Therefore, lipoamide is readily taken up by HeLa cells (reaching concentrations comparable to abundant cellular metabolites. It is present in a chemically unmodified form (Figure S3G,H). This concentration is one order of magnitude higher than those seen to affect FUS GFP condensates *in vitro* indicating a physicochemical effect in cells is plausible.

Lipoamide/lipoic acid prevents stress granule protein aggregation *in vivo*

As lipoamide and lipoic acid had a large effect on FUS aggregation *in vitro* we used a filter-trap retention assay (in which aggregated protein from cell lysate tends to be retained on a membrane)[52] to test whether lipoamide had a beneficial effect on spontaneous aggregation of wild-type or P525L FUS GFP in iPSCs (Figure S4). Both cell lines had evidence for some FUS aggregation, which was reduced following treatment with lipoamide (Figure S4B).

To look for evidence of *in vivo* effects on stress granule formation and protein aggregation we turned to *Caenorhabditis elegans.* In *C. elegans*, ageing or chronic stress are associated with aggregation of stress granule proteins with an LCD/RBP domain structure (including the orthologs of TIAL1 and PABC1)[53]. This has parallels with the observation of aggregated stress granule proteins in ALS pathogenesis. Notably, *C. elegans* grown in liquid culture with R-(+) or S-(−)-lipoic acid showed a dose-dependent decrease in the proportion of animals with aggregation of PAB-1 (Figure 8A,B), the ortholog of PABC1 (analysed in HeLa cells in Figure 4C). At the highest concentration tested (2 mM) there was some toxicity leading to 6 to 8% worm death. Testing of lipoamide was not possible due to precipitation in the worm culture medium.

To investigate whether this action of lipoic acid is specific to RBPs with LCDs, we tested the aggregation of two globular proteins KIN-19 and RHO-1, which have been previously shown to aggregate with age in *C. elegans*[54]. Neither protein has an RNA-binding domain or LCD. We found no effect of 1.5 mM lipoic acid on RHO-1 aggregation and a slight decrease in KIN-19 aggregation (Figure 8A). Thus, lipoic acid can affect stress granule solidification *in vivo* on the timescale of an organism lifespan, correlating with its behavior on short time scales *in vitro*. This is consistent with its direct interaction with stress granule proteins to reduce stress granule formation and/or stress granule protein aggregation.

Lipoamide/lipoic acid recover neuron and organism FUS-associated defects

P525L is a well-characterised example of an ALS-associated FUS NLS mutation and iPSC-derived motor neurons (iPSC MNs) expressing P525L from ALS patients show defects consistent with motor neuron defects in the patient[46]. iPSC MNs can be grown through silicone channels, positioning the soma on one side with the axons protruding through the channels to the far side. Such cultures can be maintained for long periods (>60 days). However, in this system, P525L FUS MNs exhibit cellular defects associated with neurodegeneration, including axonal die-back and reduced axonal transport. This occurs even without exogenous cell stressors, although P525L FUS MNs have a greater propensity to form stress granules[46], and has similarities to the axon retraction leading to motor dysfunction in ALS patients.

We therefore tested whether lipoamide or lipoic acid was able to improve these phenotypes. FUS P525L neurons initially appear morphologically normal (Figure 8D) but by 60 days in culture died-back axonal material has accumulated around the exit of neurons from the silicone channels (Figure 8D). Inclusion of 2 µM lipoic acid or lipoamide in the culture medium prevented the die-back (Figure 8C-E). As defective axonal transport is thought to lead to axon die-back[55] we analysed the transport of lysosomes within the axons of iPS MNs expressing P525L FUS with or without lipoamide in

comparison to iPS MNs expressing WT FUS (Figure 8F). Lipoamide recovered axonal transport in P525L FUS iPS MNs to the same level as WT neurons. This is a greatly beneficial effect of lipoamide in a minimal *ex vivo* model using human cells in a long-term treatment regime. As no stressor is needed to induce axon die back, we suggest that lipoic acid either helps iPSC MNs handle stochastic stress in culture or facilitates the amelioration of a defect caused by P525L.

Next, we tested whether lipoic acid could have a similar beneficial effect on motor neurons *in vivo* using a fly model. The *Drosophila menalogaster* FUS ortholog, cabeza, is required for normal neuronal development[56]. FUS has a longer N terminal prion-like LCD than cabeza and expression of human FUS in *D. menalogaster* causes motor defects, including a reduced ability to climb. Expression of P525L or R521C human FUS (both of which are NLS mutants) causes even more severe motor defects. Food supplementation with either lipoamide (Figure 8G) or lipoic acid (Figure 8H) successfully recovered motor defects in flies expressing P525L or R521C FUS, increasing the proportion of flies able to climb 4 cm in 30 s from ~50% to >80%. This significant restoration of the flies' ability to climb indicates both compounds are capable of recovering motor neuron defects caused by FUS.

Discussion

In this paper, we identify lipoamide and lipoic acid as promising therapeutics for ALS. These compounds have a long and complex history as bioactive molecules however their mechanism of action is ambiguous. Stress granules have been proposed to be crucibles of ALS pathogenesis[6] therefore we screened for compounds that affect the physical chemistry of a model stress granule protein, FUS. Here, we showed lipoamide altered the properties of phase separated FUS condensates *in vitro* (Figure 6A,B), reduced stress granule formation and promoted a return of FUS to the nucleus in stressed cells (Figure 3,4), reduced aggregation of FUS in vitro and in cells (Figure 6C-H,S4), reduced aggregation of stress granule proteins in animals (Figure 8A,B) and ameliorated pathological phenotypes in neurons and animals linked with expression of FUS mutants associated with familial ALS (Figure 8C-H). Lipoic acid has previously shown some efficacy in SOD1 animal models of ALS[57,58] and our work shows efficacy in models of stress granule protein-driven ALS pathogenesis through a novel mechanism of action.

Stress granules form by phase separation of proteins within the cytoplasm and a few small molecules have previously been identified which modulate phase separation (notably 1,6-hexanediol), however lipoic acid and lipoamide have far more plausibility as a therapeutic. Concentrations of 1,6-hexanediol between 1 to 10% (several hundred mM) are required for *in vitro*

or cellular activity, and this is rapidly toxic[23,25]. The molecules we identified in our screen (both heterotri- and tetracyclic compounds and lipoamide and related compounds) were active *in vitro* (Figure 2,6) and on cells (Figure 1,3,S1) at vastly lower concentrations (tens to hundreds of µM), three to four orders of magnitude lower than 1,6-hexanediol. The effect of lipoamide on stress granules is also specific, in the sense that lipoamide did not affect other membraneless liquid like compartments in cells – it did not affect nuclear compartments formed by FUS (Figure 5B) or formed by other proteins either in the cytoplasm or nucleus (Figure 5A) and was well-tolerated by HeLa, iPS and motor neuron cells in culture.

The necessary properties of a compound affecting protein phase separation are likely different to those of a canonical drug binding a well-defined structured protein site. Condensates are formed by protein liquid-liquid phase separation involving many transient interactions[59], unlike strong enzyme-substrate or protein-protein interactions typically targeted by drugs. Small molecules can interfere with phase separation and alter the properties of phase boundaries (surfactants). For instance, ATP has been identified as a hydrotrope which helps keep proteins soluble[60]. The identification of lipoamide and lipoic acid suggests that further small molecules could be identified that target phase separated compartments.

While lipoamide and lipoic acid are commonly viewed as antioxidants, our evidence indicates they have activity outside of classical antioxidant effects on FUS *in vitro* and stress granules in cells. *In vitro* we observed multiple effects of lipoamide/lipoic acid on FUS condensates in the presence of an excess of reducing agent (Figure 6). In the cell, lipoamide/lipoic acid are also unlikely to play part of a redox cycle as lipoamide dehydrogenase has much greater activity on the R-(+) isomer[43], but we saw a similar EC_{50} for lipoic acid isomers on cells (Figure 3) and saw similar activity of both isomers on neurons and in *C. elegans* (Figure 8). A direct effect on stress granules involving modulation of their physical chemistry is therefore plausible. However, it is important to point out that the nature of this interaction may involve redox interaction with the thiol groups.

In cells, lipoamide caused dissolution of stress granules formed under several cellular stresses (Figure 4), while *in vitro* lipoamide did not cause dissolution of FUS condensate droplets (Figure 6), appearing to affect the kinetics rather than thermodynamics of FUS phase separation. One likely reason is that lipoamide accumulates to remarkably high concentrations in cells (Figure 7) where it is likely reduced but is not otherwise metabolised (Figure S3). The estimated cellular concentration (approximately 5 mM) is one order of magnitude higher than we were able to reach *in vitro* (300 µM), and much higher than the concentration necessary to increase the liquidity and reduce the hardening of phase separated FUS *in vitro* (Figure 6), however it may also affect cell volume

through osmotic effects. It is possible that 5 mM lipoamide would dissolve FUS condensate droplets *in vitro*. There are also other potential explanations. Firstly, higher liquidity of stress granules could make them more sensitive to cellular stress granule dissolving factors. Secondly, that cells have stress granule, cytoplasm and nuclear environments, making it a more complex three phase system (perhaps related to the lipoamide effect on FUS nuclear/cytoplasm partition, Figure 3). Finally, lipoamide has a strong effect on the solidification of FUS (Figure 6), and this is thought to be driven in part by LCD-LCD interactions that are not required for phase separation *in vitro*[26]. If LCD-LCD interactions are more important for phase separation inside cells then this may manifest as an increased sensitivity stress granules to lipoamide relative to FUS *in vitro*.

The cellular target of lipoamide or lipoic acid could not be unambiguously confirmed. While these compounds alter the properties of FUS condensates *in vitro*, FUS is not vital for stress granule formation. Therefore FUS cannot be the only cellular target. Many stress granule proteins are FUS-like with LCD domains and were affected in cells by treatment, including G3BP1, which is thought to nucleate stress granules (Figure 4). Lipoamide and lipoic acid may be affecting a shared property of several FUS-like stress granule proteins or a key vital stress granule protein. If a physical chemistry mechanism is correct, we anticipate lipoamide modulates transient and weak interactions between FUS molecules to modulate condensate properties instead of having a single binding site. It is perhaps unsurprising that NMR was unable to detect an interaction (Figure S2) despite a clear effect on the physical properties of FUS condensates *in vitro* (Figure 6). The caveats are that this assay concerned only the FUS LCD in the non-phase separated phase – lipoamide could interact with other regions of FUS such as the RNA binding domain absent in this assay. Overall we were unable to provide orthogonal evidence of compound/stress granule protein interaction in cells.

The utility of lipoamide/lipoic acid as a therapeutic presumably depends on the balance between stress granules promoting ALS pathogenesis and stress granule formation as a beneficial cellular response to stress. Similarly, whether stress granule protein aggregation is a means of sequestering a harmful protein, whether it is intrinsically harmful, or if it is detrimental to other (for example, nuclear[46]) stress granule protein functions. The strong association of FUS NLS mutations and the capacity for nuclear import of FUS with ALS gives particular plasubility to the latter[39,40,46,61]. Our motor neuron and *D. melanogaster* models of ALS showed that the pattern of action of lipoamide and lipoic – dissolving stress granules, returning FUS to the nucleus, not affecting FUS recruitment to DNA damage and not affecting other compartments – was beneficial. In humans, a 600 mg daily dose of lipoic acid gives plasma concentrations of 8 to 30 µM, comparable to the concentrations used in our cell-based assays, suggesting that lipoic acid has surprising plausibility as a therapeutic.

We were unable to unambiguously link the short time-scale effects of lipoamide/lipoic acid on cells and purified protein to the longer time-scale effects on motor neurons, *C. elegans* stress granule protein aggregation and *D. melanogaster* motor function. There is evidence that lipoamide and lipoic acid promote mitochondrial biogenesis[62,63] as part of longer timescale 'indirect' antioxidant effects[64]. These mechanisms do not plausibly contribute to the short timescale cell-based assays, but are likely to contribute to the effects of long-term lipoamide/lipoic acid treatment. This is important, as there are strong links with mitochondrial health and ALS[65]. However, we saw that lipoamide and lipoic acid could recover pathology caused by expression of FUS NLS mutants which have no direct link to mitochondrial biology (Figure 8). One possibility is that lipoamide improves mitochondrial health and helps cells overcome the FUS-associated defect. Alternatively, lipoamide modulates cellular stress responses overcoming the FUS-associated defect and leading to improved mitochondrial health. It is notable that lipoamide, on dissolution of stress granules, promotes a return of FUS to the nucleus, which may be a key upstream mechanism for FUS NLS mutant pathology[46], however at this time there is not enough clarity concerning the precise mechanisms of ALS pathogenesis exactly which lipoamide effect is beneficial. Nonetheless our assays show that lipoamide and lipoic acid are non-toxic and effective in long-term treatment of ALS patient-derived neurons.

It has recently become clear that many important cellular compartments are biomolecular condensates formed by phase separation of different intrinsically disordered proteins (IDPs) (ref). Stress granules are just one example, and many other condensates are also linked to disease. This places our question of whether it is possible to interfere with the physical of stress granule formation using small molecules within a wider question of whether phase separation of IDPs is a possible drug target. Targeting individual IDPs associated with disease is not feasible as many proteins are implicated in a single neurodegenerative disease. Analogously, within ALS, many different mutations cause pathology and it is likely not feasible to target each mutation separately. We have shown that compounds which affect phase separation can be found and are beneficial. This points to a new class of drugs – affecting the physical chemistry of phase separating proteins– and suggests the term physicochemical drug. Perhaps the solution to protein aggregation in disease is to support the cell's ability to maintain a dissolving environment, and future screens may identify further small molecule able to do so.

Methods

Stable Kyoto HeLa BAC cell lines expressing proteins with a C-terminal GFP fluorescent marker were generated using BAC recombineering[45]. This gives near-endogenous expression level of the fusion

protein[7,66]. In these lines, GFP is part of a modified localisation and affinity purification (LAP) tag[67], providing a short linker. HeLa cells were grown in high glucose DMEM supplemented with 10% FCS. Cultures were supplemented with 1% penicillin-streptomycin, and maintained under Geneticin (Gibco, 400 µg/ml) selection at 37°C with 5% CO_2.

Human iPS cells lines, derived from three different donors, expressing FUS with a C-terminal GFP fluorescent marker were used. All were generated using CRISPR/Cas9 assisted tagging and mutagenesis and have been previously described[46,68]. In summary: JS-SL-C1 iPS cells expressing either wild-type or P525L FUS GFP[68] were previously generated from a healthy female donor[69]. JS-SL-C1 iPS cells were used for used for compound dose response analysis. KOLF iPS cell lines expressing wild-type FUS GFP or P525L FUS GFP were previously generated from the KOLF-C1 clonal iPS cell line produced as part of the human induced pluripotent stem cell initiative (HipSci)[70]. KOLF-C1 cells were derived from a healthy male donor. In these lines, GFP is part of a modified localisation and affinity purification (LAP) tag[67], providing a short linker and giving an identical fusion protein sequence to the Koyoto HeLa BAC cell line. JS-SL-C1 and KOLF-C1 iPS cell lines were used as an isogenic pair for analysis of DNA damage response and lipoamide action on P525L FUS. AH-ALS1-F58 iPS cell expressing P525L FUS with a C-terminal GFP fluorescent marker were previously generated from a clonal iPS cell line from a female ALS patient expressing P521C FUS. The P525L mutation and GFP tag were introduced and the P521C mutation corrected by simultaneous tagging and mutagenesis[46,71,72]. iPS cells were grown in TeSR E8 medium (Stem Cell Technologies) at 37°C with 5% CO_2[69,73,74].

MNs were generated from AH-ALS1-F58 iPS cells expressing P525L FUS in Matrigel coated plates with silicone channels for axons by inducing differentiation as previously described[74]. This yields clusters of soma on one side of the channels with axons which extend through the channels and protrude out of the far side of the channels. AH-ALS1-F58 were used to generate motor neurons (MNs) as they have previously been characterised in axonal transport assays[46]. iPS MNs used for assays within 4 weeks of the completion of differentiation, unless otherwise stated.

All procedures using human cell samples were in accordance with the Helsinki convention and approved by the Ethical Committee of the Technische Universität Dresden (EK45022009, EK393122012).

Recombinant protein

For *in vitro* condensate formation screening and solidification assays recombinant GFP FUS and GFP G156E FUS were purified using baculovirus/insect cell expression system, exactly as previously described[7]. Briefly, His MBP FUS GFP was purified from cell lysate by Ni-NTA affinity purification, the

His MBP cleaved, then concentrated by dialysis and further purified by size exclusion chromatography. The composition of the storage buffer for purified FUS was 1M KCl, 50 mM Tris·HCl pH 7.4, 5% glycerol and 1 mM DTT, and FUS concentration was adjusted to 30 µM in storage buffer prior to use.

Compounds

For *ex vivo* and *in vitro* screens the PHARMAKON 1600 library was used, prepared as 10 mM stocks in DMSO. For follow-up assays, compounds were repurchased and prepared as 10 mM stocks in DMSO; lipoamide (T5875, Sigma Aldrich or sc-239160, Santa Cruz Biotechnology), lipoic acid (62320, Sigma Aldrich), R-(+)-lipoic acid (07039, Sigma Aldrich), S-(−)-lipoic acid (08561, Sigma Aldrich), dihydrolipoic acid (T8260, Sigma Aldrich), valeric acid (240370, Sigma Aldrich), 1,3-propanedithiol (P50609, Sigma Aldrich), mitoxantrone (M6545, Sigma Aldrich), N-(2-hydroxyethyl)ethylenediamine (127582, Sigma Aldrich), 1,4-dihydroxyanthraquinone (Q906, Sigma Aldrich), cetylpyridinium chloride (C9002, Sigma Aldrich), quinacrine (Q3251, Sigma Aldrich), 9-aminoacridine (A38401, Sigma Aldrich), 2-amino-5-diethylaminopentane (A48806, Sigma Aldrich), daunorubicin (30450, Sigma Aldrich), 8-acetyl-6,11-dihydroxy-7,8,9,10-tetrahycro-napthacene-5,12-dione (R162892, Sigma Aldrich). ^{15}N racemic and R-(+)-lipoamide were synthesised (see Supplementary Information) and characterised by ^{1}H NMR, ^{13}C NMR, mass spectrometry, infrared spectroscopy and melting point. Yield was ~50%, with ^{15}N label at ~99%.

Ex vivo HeLa cell screen

The effect of compounds on FUS GFP localisation in stressed HeLa cells was screened in 384 well format. 4000 cells were seeded per well and incubated for 24 h, after which the medium was replaced with 40 µl fresh medium and compound added to a final concentration of 10 µM by acoustic dispensing (Labcyte Echo 550). The final concentration of DMSO in all samples was 0.1%. After 1 h potassium arsenate was added from a 5× stock solution to a final concentration of 1 mM and the cells incubated a further 1 h, then the cells were fixed with 7.4% formaldehyde, stained with 1 mg/ml Hoechst 33342 and 1:10,000 CellMask blue (ThermoFisher). Six fields of view per well were captured using a CellVoyager CV7000 automated spinning disc confocal microscope (Yokogawa) using a 40× NA 1.3 water immersion objective. Each plate included 48 wells treated with 0.1% DMSO and stressed with arsenate (compound solvent control), along with 8 untreated unstressed wells and 4 unstressed untreated wells with parental Koyoto HeLa cells. All images are displayed at gamma 0.7 to show bright stress granules and faint nuclei simultaneously.

For the initial screen FUS GFP signal was analysed using KNIME[75]. Cytoplasm was identified from weak (CellMask blue), and nuclei from strong (Hoechst 33342) blue fluorescent signal. Particle number and sum area, granularity at 9, 10 & 11 px (cytoplasm) or 1, 5, 6, 7, 8 & 9 px (nucleus) scale, texture at 10 px scale and integrated signal intensity were measured for the nucleus and cytoplasm in the green (FUS GFP) channel. Z scores ($z = (x - \mu)/\sigma$ where x is the observed value, μ the control mean and σ the control standard deviation) relative to the DMSO treated control wells on each plate were calculated for each of the parameters and combined into the Mahalanobis distance.

In vitro purified FUS GFP screen

The effect of compounds on FUS GFP condensates *in vitro* was assessed in 384 well plate format. The compound volume (in DMSO) necessary for 1, 3, 10, 30 or 100 µM final concentration were added by acoustic dispensing (Labcyte Echo 550) to 96 well plate wells containing 3 µl FUS GFP diluted in 50 mM Tris·HCl pH 7.4, 1 mM DTT (for low salt assays). Final DMSO concentration was 0.01 to 1%. Using a Freedom Evo 200 liquid handling workstation (TECAN) the FUS GFP/compound mixture was diluted in 7 µl assay buffer containing 50 mM Tris·HCl pH 7.4, 1 mM DTT, 50mM KCl and 0.7 µM FUS GFP. Compound/FUS GFP and assay buffer were mixed by a standardised pipetting procedure then split to four wells in clear bottom 384 well plates then immediately imaged using a CellVoyager CV7000 automated spinning disc confocal microscope (as above). Condensates in suspension for six fields of view were imaged as a maximum intensity projection of 6 focal planes at 2 µm steps per sample. Condensate number and FUS GFP partition into condensates were analysed with a fixed intensity threshold using ImageJ[76]. Number of condensates and partition were weakly time dependent due to condensate sedimentation, so normalised assuming a linear change over time by reference to DMSO controls at the start and end of each plate row.

Compound characterisation on HeLa and iPS cells

Compound effects were assessed under a variety of conditions in HeLa or iPS cells expressing wild-type or P525L FUS GFP by live cell imaging. Different combinations of 1 h pre-treatment compound or pre-stress with arsenate followed by 1 h treatment with compound and/or stress with arsenate. Unless otherwise indicated, cells were pre-treated for 1 h using 10 µM compound from 10 mM stock in DMSO (or an equal volume of DMSO control) then stressed for 1 h with 1 mM potassium arsenate still in the presence of compound. GFP fluorescence was imaged by widefield epilfluorescence using an inverted Olympus IX71 microscope with an Olympus 100× NA 1.4 Plan Apo oil immersion objective and a CoolSNAP HQ CCD camera (Photometrics), using a DeltaVision climate control unit (37°C, 5% CO_2) (Applied Precision). The kinetics of pre-stress followed by treatment was analysed

from images captured at 2 min intervals for 100 min, for single time points images were captured after 1 h unless otherwise indicated.

Various cellular stresses were achieved by replacing 1 h 1 mM potassium arsenate treatment with other conditions: 100 µM rotenone (R8875, Sigma Aldrich) from a 1 M stock in DMSO for 2 h (mitochondrial stress). Serum-free DMEM for 2.5 h (serum starvation stress). Sorbitol (S1876, Sigma Aldrich) from a 4 M stock in H_2O for 1 h (osmotic stress). 42°C in normal growth medium for 30 m (heat stress). 100 mM 6-deoxyglucose (D9761, Sigma Aldrich) from a 1 M stock in H_2O in glucose free DMEM (11966025, ThermoFisher Scientific) supplemented with 10% FCS for 1 h (glycolysis stress). Appropriate solvent controls were used.

For Western blots and analysis of intracellular FUS aggregates iPS cells were lysed with RIPA buffer. Western blots were performed using standard methods and the following antibodies: Mouse anti-FUS (AMAB90549 Sigma Aldrich, 1:500 dilution), rabbit anti-GFP (sc-8334 Santa Cruz, 1:400) or rabbit anti-GAPDH (2118S NEB, 1:5000) primary antibody with horseradish peroxidase-conjugated anti-mouse or anti-rabbit (Dianova 1:10,000) secondary antibodies. The filter retardation assay for intracellular FUS aggregates was performed as previously described[52]. Briefly, protein extracts were loaded on 0.2 µm cellulose acetate membrane then subject to microfiltration, leaving aggregated protein on the membrane. Aggregated FUS was detected as above.

HeLa cell compound dose responses

Dose dependent effect of compounds on HeLa or iPS cells expressing FUS GFP were assessed using 1 h 1 mM potassium arsenate stress as for the *ex vivo* HeLa cell screen, except serial compound dilutions in medium were prepared manually from 80 µM to ~0.4 nM at 1.189× dilution steps. Small dilution steps rather than concentration replicates were selected as it provides greater statistical power from a set number of samples[77]. Final DMSO concentration was 0.08% in all samples, and each plate included at least 12 control wells with 0.08% DMSO. Cytoplasmic FUS condensate number and nuclear/cytoplasm partition of FUS were analysed using custom macros in ImageJ[76]. Nuclei were identified by intensity thresholding of the blue fluorescence image following a 5 px Gaussian blur. Cytoplasmic FUS condensates by intensity thresholding of the green image following a 10 px weight 0.9 unsharp filter masked by the thresholded nuclei, and nuclear FUS condensates by intensity thresholding of the green image following a 5 px weight 0.9 unsharp filter and 10 px rolling ball background subtraction masked to only include thresholded nuclei. The ratio of cytoplasmic FUS condensates to nuclei was taken as cytoplasmic FUS condensates per cell per field of view, and p, the ratio of partition of FUS to the nucleus and the cytoplasm, was derived from $a = v_n/v_t$, the ratio of nuclear to total green signal per field of view, where $p = a/(1-a)$. These data were log

transformed and fitted to a Rodbard sigmoidal curve[78] to determine EC_{50}. Six fields of view were captured and analysed per condition.

In vitro FUS GFP solidification assays

For *in vitro* solidification assays, FUS GFP in storage buffer was diluted in water to give 10 µM FUS, 50 mM Tris·HCl pH 7.4 and 1 mM DTT in a 20 µl volume in non-binding clear bottom 384 well plates (Greiner Bio-One, 781906). Compounds, or an equal volume of DMSO, were then added for a final compound concentration of 30 µM and 0.3% DMSO. 'Aging' to cause fibre was induced by horizontal shaking at 800 rpm at room temperature, similar to as previously described[7]. Fibre and condensate formation were analysed by widefield epifluorescence using a DeltaVision Elite microscope (GE Healthcare Life Sciences) with a Plan ApoN 60× NA 1.4 oil immersion objective (Olympus) and an sCMOS camera (PCO). For salt sensitivity of condensate formation FUS GFP in storage buffer was diluted in the appropriate concentration of KCl pre-mixed with compound or DMSO to generate the final KCl concentration series with 30 µM compound concentration and 0.3% DMSO.

Fluorescence recovery after photobleaching (FRAP) of FUS GFP condensates and fibres was performed on a Nikon TiE inverted microscope with a Nikon Apo 100× NA 1.49 oil immersion objective using a Yokogawa CSU-X1 spinning disc head and an Andor iXon EM+ DU-897 EMCCD camera. 10×10 px regions were bleached for 50 ns with a 6 mW 405 nm laser using an Andor FRAPPA beam delivery unit then imaged for 5 min at 5 Hz. Recovery curve half-life and mobile fraction were calculated in ImageJ[76].

Ex vivo DNA cut assays

UV micro-irradiation of live cells to induce DNA damage was performed as previously described[7]. KOLF iPS MNs expressing wild-type GFP were stressed by addition of 1 mM potassium arsenate for 1 h, then were treated with lipoamide, mitoxantrone or an equal volume of DMSO for 1 h. A single point in the nucleus was subject to 3 UV pulses as described for FRAP, but at 10% laser power. GFP fluorescence was imaged at 1 Hz, and intensity of response was analysed in ImageJ[76].

NMR

For analysis of compound interaction with FUS untagged FUS low complexity domain (residues 1 to 163) expressed, purified and analysed using ^{1}H-^{15}N heteronuclear single quantum coherence NMR and sample conditions previously described[18] in the presence of 500 µM compound or equivalent DMSO solvent control (1%).

For analysis of ^{15}N lipoamide uptake by cells HeLa cells expressing FUS GFP were grown in 6 well plates to 10^6 cells/well in DMEM supplemented with 10% FCS. To simultaneously stress and treat

cells, the medium was replaced with 0.6 ml medium supplemented with potassium arsenate and 100 µM ^{15}N racemic or R-(+)-lipoamide for 1 h at 37°C. High concentrations of compound were used to maximise the signal. The medium was then removed and retained (medium sample), the cells washed with ~2 ml PBS, then the cells removed by trypsinisation: Addition of 0.3 ml TrypLE Express (12604013, ThermoFisher) and incubation at 37°C for 5 min, then addition of 0.3 ml medium to quench the trypsin. The resuspended cells were retained (cell sample). All samples were frozen at -80°C. Wells were prepared for all combinations of no compound (1% DMSO control), ^{15}N (±)-lipoamide or ^{15}N R-(+)-lipoamide, with or without potassium arsenate and with or without cells. ^{1}H detected ^{15}N edited ^{1}H sensitivity enhanced HSQ was used to quantify ^{15}N lipoamide concentration (see Supplementary Information). Solvent, pH and temperature sensitivity of the primary amide proton chemical shifts were determined using dummy samples assembled from the appropriate solvent and added compounds.

Neuron dieback and axonal transport assays

For analysis of axon dieback transport AH-ALS1-F58 iPS MNs expressing P525L FUS or an isogenic control expressing WT FUS were grown with 2 µM compound or an equal volume of DMSO for 60 days. Over this length of culture neurons expressing WT FUS have stable axons, while neurons expressing P525L FUS do not. Axon dieback is visible as accumulated cell detritus at the exit of axons from channels. Experiments and analysis were performed blinded, and axonal dieback was scored qualitatively using phase contrast images captured every 10 to 20 days.

For analysis of axonal transport iPS MNs expressing P525L FUS were treated with 2 µM compound or an equal volume of DMSO for 3 days. Longer incubation was selected to ensure penetration and action of compounds along the length of the axon channel. 2 µM was selected as the highest concentration where there were no toxic effects (assessed qualitatively). Analysis of axonal transport of liposomes were performed as previously described[46]. Briefly, liposomes were labelled by addition of 50 nM lysotracker red (ThermoFisher) and imaged using a Leica DMI6000 inverted microscope with a 100× NA 1.46 oil immersion objective and an Andor iXON 897 EMCCD camera in an incubator chamber (37°C, 5% CO_2) at 3⅓ Hz for 120 s at either the proximal or distal end of the silicone channels containing the axons.

Particle tracking was used to identify proportion of particles moving faster than 0.2 µm/s for five videomicrographs. Each video includes a variable population of non-moving background particles, therefore, for each biological replicate, data were normalised to the mean proportion of fast moving lysosomes in the DMSO (solvent control) treated FUS P525L samples.

Protein aggregation in *C. elegans*

The effect of lipoic acid on stress granule protein aggregation *in vivo* was analysed using a *C. elegans* model for stress granule formation and aggregation. As previously described[53,79], fluorescent-tagged PAB-1 forms abundant stress granules and large solid aggregates during aging or upon chronic stress. RHO-1 and KIN-19 also aggregate during aging, but are not RNA binding or stress granule proteins. Three lines were used: Fluorescently tagged PAB-1 (DCD214: N2; *uqIs24[pmyo-2::tagrfp::pab1gene]*), KIN-19 (CF3649: *N2; muIs209[pmyo-3::kin-19::tagrfp+ptph-1::GFP]* and RHO-1 (DCD13: N2; *uqIs9[pmyo-2::rho-1::tagrfp+ptph-1::gfp]*). Each were analysed as below, except DCD13 were maintained at at 20°C.

The animals were exposed to lipoic acid in liquid culture in a 96 well plate starting from larval stage L4 in a total volume of 50 µl S-Complete per well (100 mM NaCl, 50 mM Potassium phosphate pH 6, 10 mM potassium citrate, 3 mM $MgSO_4$, 3 mM $CaCl_2$, 5 µg/mL cholesterol, 50 µM ethylenediaminetetraacetic acid (EDTA), 25 µM $FeSO_4$, 10 µM $MnCl_2$, 10 µM $ZnSO_4$, 1 µM $CuSO_4$) supplemented with heat-killed OP50 and 50 µg/ml carbenicillin. Per experiment, a minimum of nine wells each with 13 animals were treated with R-(+) or S-(−)-lipoic acid or an equivalent volume of DMSO. Toxicity (data not shown) was evaluated from the number of dead or aberrantly small-sized animals.

48h after switching the L4s from 20°C to 25°C (day 2 of adulthood) extensive aggregation of fluorescently tagged PAB-1 and RHO-1 occurs in the pharyngeal muscles and KIN-19 throughout the animal. After immobilization with 2 mM levamisole aggregation was scored using a fluorescent stereo microscope (Leica M165 FC, Plan Apo 2.0× objective). For PAB-1, aggregates occurred primarily in the terminal bulb of the pharynx and aggregation was scored as high (>10 aggregates per animal) or low (<10). For RHO-1, aggregates were scored in the isthmus of the pharynx and aggregation was scored as high (>50% of the isthmus), medium (<50%) or low (no aggregation). For KIN-19 aggregates occurred throughout the body wall muscles and aggregation was scored as high (aggregates in the head, middle body and tail), medium (>15 aggregates in the head and middle body) or low (>15 aggregates in the head or middle body).High-magnification images were acquired with a Leica SP8 confocal microscope with a HC Plan Apo CS2 63× NA 1.40 oil objective using a Leica HyD hybrid detector. tagRFP::PAB-1 was detected using 555nm as excitation and an emission range from 565-650nm. Representative confocal images are displayed as maximum z stack projection.

Motor defects in *D. melanogaster*

All Drosophila stocks were maintained on standard cornmeal at 25°C in light/dark controlled incubator. The w1118, UAS-eGFP, and D42-GAL4 were obtained from Bloomington stock center. The UAS-FUS WT, UAS-FUS P525L, and UAS-FUS R521C were previously described[80].

Climbing assays were performed as previously described[80]. Briefly, flies expressing FUS, eGFP or w1118 were grown in the presence or absence of (±)-α-Lipoic Acid (0.43mM or 2.15mM diluted in ethanol), (R)-(+) -α-Lipoic Acid (0.43mM or 2.15mM diluted in ethanol), (S)-(-) -α-Lipoic Acid (0.43mM diluted in ethanol), (±)-α-Lipoamide (0.43mM diluted in DMSO), or PP 242/Torkinib (10µM or 50µM diluted in DMSO), then anesthetised, placed into vials and allowed to acclimatise for 15 mins in new vials. For each fly genotype, the vial was knocked three times on the base on a bench and a video camera was used to record the flies climbing up the vial walls. The percentage of flies that climbed 4 cm in 30 s was recorded. Statistical analysis was carried out in GraphPad Prism 6 using either Student's T-test or one-way ANOVA with Tukey's or Dunnet's multiple comparisons test.

Acknowledgements

The Wheeler lab is supported by the Wellcome Trust [211075/Z/18/Z, 103261/Z/13/Z]. The Hermann lab is supported by the NOMIS foundation, the Helmholtz Virtual Institute "RNA dysmetabolism in ALS and FTD (VH-VI-510)", an unrestricted grant by a family of a deceased ALS patient, the Stiftung zur Förderung der Hochschulmedizin in Dresden and the Hermann und Lilly Schilling-Stiftung für medizinische Forschung im Stifterverband. The Fawzi lab is supported by funding from the National Institute of General Medical Sciences (NIGMS) of the National Institutes of Health (R01GM118530). NMR data was obtained at the Brown University Structural Biology Core Facility supported by the Division of Biology and Medicine, Brown University. Anastasia Murthy is supported by an NIGMS training (T32GM07601) and a National Science Foundation Graduate Research Fellowship (1644760). The David lab is supported by the Deutsches Zentrum für Neurodegenerative Erkrankungen (DZNE). The Alberti lab is supported by the European Union's Horizon 2020 research and innovation program (643417). The Sterneckert lab is supported by the Deutsche Forschungsgemeinschaft Center (DFG) Research Center (DFG FZT 111) and Cluster of Excellence (DFG EXC 168)). Both are supported by the Bundesministerium für Bildung und Forschung (01ED1601A, 01ED1601B). This is an EU Joint Programme – Neurodegenerative Disease Research (JPND) project. The project is supported through the following funding organizations under the aegis of JPND – www.jpnd.eu (Germany, Bundesministerium für Bildung und Forschung; Israel, Ministry of Health; Italy, Ministero dell'Istruzione dell'Università e della Ricerca; Sweden, Swedish Research Council; Switzerland, Swiss

National Science Foundation). Lara Marrone is supported by a Hans und Ilse Breuer Stiftung fellowship. The Fawzi lab is supported by funding from the National Institute of General Medical Sciences (NIGMS) of the National Institutes of Health (R01GM118530) and the National Science Foundation (1845734).

Conflict of interest statement

A.A.H. and S.A. are shareholders and consultants for Dewpoint Therapeutics and R.J.W has a consultancy agreement with Dewpoint. A patent application has been submitted by Dewpoint and the Max Planck Institute of Molecular Cell Biology and Genetics based on these results.

References

1. Robberecht, W. & Philips, T. The changing scene of amyotrophic lateral sclerosis. *Nat. Rev. Neurosci.* **14**, 248–264 (2013).
2. Chen, S., Sayana, P., Zhang, X. & Le, W. Genetics of amyotrophic lateral sclerosis: an update. *Mol. Neurodegener.* **8**, 28 (2013).
3. Miller, R. G., Mitchell, J. D. & Moore, D. H. Riluzole for amyotrophic lateral sclerosis (ALS)/motor neuron disease (MND). *Cochrane Database Syst. Rev.* CD001447 (2012). doi:10.1002/14651858.CD001447.pub3
4. Writing Group & Edaravone (MCI-186) ALS 19 Study Group. Safety and efficacy of edaravone in well defined patients with amyotrophic lateral sclerosis: a randomised, double-blind, placebo-controlled trial. *Lancet Neurol.* **16**, 505–512 (2017).
5. Deng, H., Gao, K. & Jankovic, J. The role of FUS gene variants in neurodegenerative diseases. *Nat. Rev. Neurol.* **10**, 337–348 (2014).
6. Li, Y. R., King, O. D., Shorter, J. & Gitler, A. D. Stress granules as crucibles of ALS pathogenesis. *J. Cell Biol.* **201**, 361–372 (2013).
7. Patel, A. *et al.* A Liquid-to-Solid Phase Transition of the ALS Protein FUS Accelerated by Disease Mutation. *Cell* **162**, 1066–1077 (2015).
8. Nomura, T. *et al.* Intranuclear aggregation of mutant FUS/TLS as a molecular pathomechanism of amyotrophic lateral sclerosis. *J. Biol. Chem.* **289**, 1192–1202 (2014).
9. Aulas, A. & Vande Velde, C. Alterations in stress granule dynamics driven by TDP-43 and FUS: a link to pathological inclusions in ALS? *Front. Cell. Neurosci.* 423 (2015). doi:10.3389/fncel.2015.00423
10. Protter, D. S. W. & Parker, R. Principles and Properties of Stress Granules. *Trends Cell Biol.* **26**, 668–679 (2016).
11. Alberti, S. & Carra, S. Quality Control of Membraneless Organelles. *J. Mol. Biol.* **430**, 4711–4729 (2018).
12. Johnson, B. S. *et al.* TDP-43 is intrinsically aggregation-prone and ALS-linked mutations accelerate aggregation and increase toxicity. *J. Biol. Chem.* jbc.M109.010264 (2009). doi:10.1074/jbc.M109.010264
13. Alberti, S. & Hyman, A. A. Are aberrant phase transitions a driver of cellular aging? *BioEssays News Rev. Mol. Cell. Dev. Biol.* **38**, 959–968 (2016).
14. Molliex, A. *et al.* Phase Separation by Low Complexity Domains Promotes Stress Granule Assembly and Drives Pathological Fibrillization. *Cell* **163**, 123–133 (2015).

15. Mackenzie, I. R. *et al.* TIA1 Mutations in Amyotrophic Lateral Sclerosis and Frontotemporal Dementia Promote Phase Separation and Alter Stress Granule Dynamics. *Neuron* **95**, 808-816.e9 (2017).
16. Hennig, S. *et al.* Prion-like domains in RNA binding proteins are essential for building subnuclear paraspeckles. *J Cell Biol* **210**, 529–539 (2015).
17. Murakami, T. *et al.* ALS/FTD Mutation-Induced Phase Transition of FUS Liquid Droplets and Reversible Hydrogels into Irreversible Hydrogels Impairs RNP Granule Function. *Neuron* **88**, 678–690 (2015).
18. Burke, K. A., Janke, A. M., Rhine, C. L. & Fawzi, N. L. Residue-by-Residue View of In Vitro FUS Granules that Bind the C-Terminal Domain of RNA Polymerase II. *Mol. Cell* **60**, 231–241 (2015).
19. Wheeler, R. J. & Hyman, A. A. Controlling compartmentalization by non-membrane-bound organelles. *Philos. Trans. R. Soc. B Biol. Sci.* **373**, (2018).
20. Kroschwald, S. *et al.* Promiscuous interactions and protein disaggregases determine the material state of stress-inducible RNP granules. *eLife* **4**, e06807 (2015).
21. Patel, S. S., Belmont, B. J., Sante, J. M. & Rexach, M. F. Natively unfolded nucleoporins gate protein diffusion across the nuclear pore complex. *Cell* **129**, 83–96 (2007).
22. Updike, D. L., Hachey, S. J., Kreher, J. & Strome, S. P granules extend the nuclear pore complex environment in the C. elegans germ line. *J. Cell Biol.* **192**, 939–948 (2011).
23. Kroschwald, S., Maharana, S. & Simon, A. Hexanediol: a chemical probe to investigate the material properties of membrane-less compartments. *Matters* **3**, e201702000010 (2017).
24. Lin, Y. *et al.* Toxic PR Poly-Dipeptides Encoded by the C9orf72 Repeat Expansion Target LC Domain Polymers. *Cell* **167**, 789-802.e12 (2016).
25. Wheeler, J. R., Matheny, T., Jain, S., Abrisch, R. & Parker, R. Distinct stages in stress granule assembly and disassembly. *eLife* **5**,
26. Wang, J. *et al.* A Molecular Grammar Governing the Driving Forces for Phase Separation of Prion-like RNA Binding Proteins. *Cell* (2018). doi:10.1016/j.cell.2018.06.006
27. Prasanth, K. V. *et al.* Regulating gene expression through RNA nuclear retention. *Cell* **123**, 249–263 (2005).
28. Hyman, A. A., Weber, C. A. & Jülicher, F. Liquid-liquid phase separation in biology. *Annu. Rev. Cell Dev. Biol.* **30**, 39–58 (2014).
29. Hughes, M. F. Arsenic toxicity and potential mechanisms of action. *Toxicol. Lett.* **133**, 1–16 (2002).
30. Watanabe, T. & Hirano, S. Metabolism of arsenic and its toxicological relevance. *Arch. Toxicol.* **87**, 969–979 (2013).
31. Kedersha, N. *et al.* Stress granules and processing bodies are dynamically linked sites of mRNP remodeling. *J. Cell Biol.* **169**, 871–884 (2005).
32. Kosnett, M. J. The Role of Chelation in the Treatment of Arsenic and Mercury Poisoning. *J. Med. Toxicol.* **9**, 347–354 (2013).
33. Yoshida, H. *et al.* Neuroprotective Effects of Edaravone: a Novel Free Radical Scavenger in Cerebrovascular Injury. *CNS Drug Rev.* **12**, 9–20 (2006).
34. Petrov, D., Mansfield, C., Moussy, A. & Hermine, O. ALS Clinical Trials Review: 20 Years of Failure. Are We Any Closer to Registering a New Treatment? *Front. Aging Neurosci.* **9**, 68 (2017).
35. Amenta, F., Traini, E., Tomassoni, D. & Mignini, F. Pharmacokinetics of different formulations of tioctic (alpha-lipoic) acid in healthy volunteers. *Clin. Exp. Hypertens. N. Y. N 1993* **30**, 767–775 (2008).
36. Teichert, J., Hermann, R., Ruus, P. & Preiss, R. Plasma kinetics, metabolism, and urinary excretion of alpha-lipoic acid following oral administration in healthy volunteers. *J. Clin. Pharmacol.* **43**, 1257–1267 (2003).

37. McIlduff, C. E. & Rutkove, S. B. Critical appraisal of the use of alpha lipoic acid (thioctic acid) in the treatment of symptomatic diabetic polyneuropathy. *Ther. Clin. Risk Manag.* **7**, 377–385 (2011).
38. Raddatz, G. & Bisswanger, H. Receptor site and stereospecifity of dihydrolipoamide dehydrogenase for R- and S-lipoamide: a molecular modeling study. *J. Biotechnol.* **58**, 89–100 (1997).
39. Dormann, D. *et al.* ALS-associated fused in sarcoma (FUS) mutations disrupt Transportin-mediated nuclear import. *EMBO J.* **29**, 2841–2857 (2010).
40. Dormann, D. & Haass, C. TDP-43 and FUS: a nuclear affair. *Trends Neurosci.* **34**, 339–348 (2011).
41. Ghibu, S. *et al.* Antioxidant properties of an endogenous thiol: Alpha-lipoic acid, useful in the prevention of cardiovascular diseases. *J. Cardiovasc. Pharmacol.* **54**, 391–398 (2009).
42. Petersen Shay, K., Moreau, R. F., Smith, E. J. & Hagen, T. M. Is α-lipoic acid a scavenger of reactive oxygen species in vivo? Evidence for its initiation of stress signaling pathways that promote endogenous antioxidant capacity. *IUBMB Life* **60**, 362–367 (2008).
43. Pick, U. *et al.* Glutathione reductase and lipoamide dehydrogenase have opposite stereospecificities for alpha-lipoic acid enantiomers. *Biochem. Biophys. Res. Commun.* **206**, 724–730 (1995).
44. Jordan, S. W. & Cronan, J. E. A New Metabolic Link: The acyl carrier protein of lipid synthesis donates lipoic acid to the pyruvate dehydrogenase complex in escherichia coli and mitochondria. *J. Biol. Chem.* **272**, 17903–17906 (1997).
45. Poser, I. *et al.* BAC TransgeneOmics: a high-throughput method for exploration of protein function in mammals. *Nat. Methods* **5**, 409–415 (2008).
46. Naumann, M. *et al.* Impaired DNA damage response signaling by FUS-NLS mutations leads to neurodegeneration and FUS aggregate formation. *Nat. Commun.* **9**, 335 (2018).
47. Zwicker, D., Hyman, A. A. & Jülicher, F. Suppression of Ostwald ripening in active emulsions. *Phys. Rev. E* **92**, 012317 (2015).
48. Murray, D. T. *et al.* Structure of FUS Protein Fibrils and Its Relevance to Self-Assembly and Phase Separation of Low-Complexity Domains. *Cell* **171**, 615-627.e16 (2017).
49. Han, T. W. *et al.* Cell-free Formation of RNA Granules: Bound RNAs Identify Features and Components of Cellular Assemblies. *Cell* **149**, 768–779 (2012).
50. Hein, M. Y. *et al.* A human interactome in three quantitative dimensions organized by stoichiometries and abundances. *Cell* **163**, 712–723 (2015).
51. Theillet, F.-X. *et al.* Structural disorder of monomeric α-synuclein persists in mammalian cells. *Nature* **530**, 45–50 (2016).
52. Crippa, V. *et al.* Transcriptional induction of the heat shock protein B8 mediates the clearance of misfolded proteins responsible for motor neuron diseases. *Sci. Rep.* **6**, (2016).
53. Lechler, M. C. *et al.* Reduced Insulin/IGF-1 Signaling Restores the Dynamic Properties of Key Stress Granule Proteins during Aging. *Cell Rep.* **18**, 454–467 (2017).
54. David, D. C. *et al.* Widespread Protein Aggregation as an Inherent Part of Aging in C. elegans. *PLOS Biol.* **8**, e1000450 (2010).
55. Kreiter, N. *et al.* Age-dependent neurodegeneration and organelle transport deficiencies in mutant TDP43 patient-derived neurons are independent of TDP43 aggregation. *Neurobiol. Dis.* **115**, 167–181 (2018).
56. Xia, R. *et al.* Motor neuron apoptosis and neuromuscular junction perturbation are prominent features in a Drosophila model of Fus-mediated ALS. *Mol. Neurodegener.* **7**, 10 (2012).
57. Andreassen, O. A. *et al.* Effects of an Inhibitor of Poly(ADP-Ribose) Polymerase, Desmethylselegiline, Trientine, and Lipoic Acid in Transgenic ALS Mice. *Exp. Neurol.* **168**, 419–424 (2001).

58. Wang, T. *et al.* α-Lipoic acid attenuates oxidative stress and neurotoxicity via the ERK/Akt-dependent pathway in the mutant hSOD1 related Drosophila model and the NSC34 cell line of amyotrophic lateral sclerosis. *Brain Res. Bull.* **140**, 299–310 (2018).
59. Hyman, A. A., Weber, C. A. & Jülicher, F. Liquid-liquid phase separation in biology. *Annu. Rev. Cell Dev. Biol.* **30**, 39–58 (2014).
60. Patel, A. *et al.* ATP as a biological hydrotrope. *Science* **356**, 753–756 (2017).
61. Dormann, D. *et al.* Arginine methylation next to the PY-NLS modulates Transportin binding and nuclear import of FUS. *EMBO J.* **31**, 4258–4275 (2012).
62. Shen, W. *et al.* Lipoamide or lipoic acid stimulates mitochondrial biogenesis in 3T3-L1 adipocytes via the endothelial NO synthase-cGMP-protein kinase G signalling pathway. *Br. J. Pharmacol.* **162**, 1213–1224 (2011).
63. Zhao, L. *et al.* Lipoamide Acts as an Indirect Antioxidant by Simultaneously Stimulating Mitochondrial Biogenesis and Phase II Antioxidant Enzyme Systems in ARPE-19 Cells. *PLoS ONE* **10**, (2015).
64. Shay, K. P., Moreau, R. F., Smith, E. J., Smith, A. R. & Hagen, T. M. Alpha-lipoic acid as a dietary supplement: Molecular mechanisms and therapeutic potential. *Biochim. Biophys. Acta BBA - Gen. Subj.* **1790**, 1149–1160 (2009).
65. Smith, E. F., Shaw, P. J. & De Vos, K. J. The role of mitochondria in amyotrophic lateral sclerosis. *Neurosci. Lett.* (2017). doi:10.1016/j.neulet.2017.06.052
66. Hein, M. Y. *et al.* A Human Interactome in Three Quantitative Dimensions Organized by Stoichiometries and Abundances. *Cell* **163**, 712–723 (2015).
67. Cheeseman, I. M. & Desai, A. A Combined Approach for the Localization and Tandem Affinity Purification of Protein Complexes from Metazoans. *Sci STKE* **2005**, pl1–pl1 (2005).
68. Marrone, L. *et al.* Isogenic FUS-eGFP iPSC Reporter Lines Enable Quantification of FUS Stress Granule Pathology that Is Rescued by Drugs Inducing Autophagy. *Stem Cell Rep.* **10**, 375–389 (2018).
69. Reinhardt, P. *et al.* Genetic correction of a LRRK2 mutation in human iPSCs links parkinsonian neurodegeneration to ERK-dependent changes in gene expression. *Cell Stem Cell* **12**, 354–367 (2013).
70. Kilpinen, H. *et al.* Common genetic variation drives molecular heterogeneity in human iPSCs. *Nature* **546**, 370–375 (2017).
71. Japtok, J. *et al.* Stepwise acquirement of hallmark neuropathology in FUS-ALS iPSC models depends on mutation type and neuronal aging. *Neurobiol. Dis.* **82**, 420–429 (2015).
72. Higelin, J. *et al.* FUS Mislocalization and Vulnerability to DNA Damage in ALS Patients Derived hiPSCs and Aging Motoneurons. *Front. Cell. Neurosci.* **10**, (2016).
73. Lojewski, X. *et al.* Human iPSC models of neuronal ceroid lipofuscinosis capture distinct effects of TPP1 and CLN3 mutations on the endocytic pathway. *Hum. Mol. Genet.* **23**, 2005–2022 (2014).
74. Reinhardt, P. *et al.* Derivation and Expansion Using Only Small Molecules of Human Neural Progenitors for Neurodegenerative Disease Modeling. *PLOS ONE* **8**, e59252 (2013).
75. Berthold, M. R. *et al.* KNIME: The Konstanz Information Miner. in *Studies in Classification, Data Analysis, and Knowledge Organization (GfKL 2007)* (Springer, 2007).
76. Collins, T. J. ImageJ for microscopy. *BioTechniques* **43**, 25–30 (2007).
77. Dushek, O. *et al.* Antigen potency and maximal efficacy reveal a mechanism of efficient T cell activation. *Sci. Signal.* **4**, ra39 (2011).
78. Oerter, K. E., Munson, P. J., McBride, W. O. & Rodbard, D. Computerized estimation of size of nucleic acid fragments using the four-parameter logistic model. *Anal. Biochem.* **189**, 235–243 (1990).
79. Lechler, M. C. & David, D. C. More stressed out with age? Check your RNA granule aggregation. *Prion* **11**, 313–322 (2017).

80. Anderson, E. N. *et al.* Traumatic injury induces stress granule formation and enhances motor dysfunctions in ALS/FTD models. *Hum. Mol. Genet.* **27**, 1366–1381 (2018).
81. Karunanithy, G. *et al.* Harnessing NMR relaxation interference effects to characterise supramolecular assemblies. *Chem. Commun.* **52**, 7450–7453 (2016).
82. Wider, G. & Dreier, L. Measuring Protein Concentrations by NMR Spectroscopy. *J. Am. Chem. Soc.* **128**, 2571–2576 (2006).
83. Baldwin, A. J. & Kay, L. E. NMR spectroscopy brings invisible protein states into focus. *Nat. Chem. Biol.* **5**, 808–814 (2009).
84. Brügger, B. *et al.* The HIV lipidome: A raft with an unusual composition. *Proc. Natl. Acad. Sci.* **103**, 2641–2646 (2006).

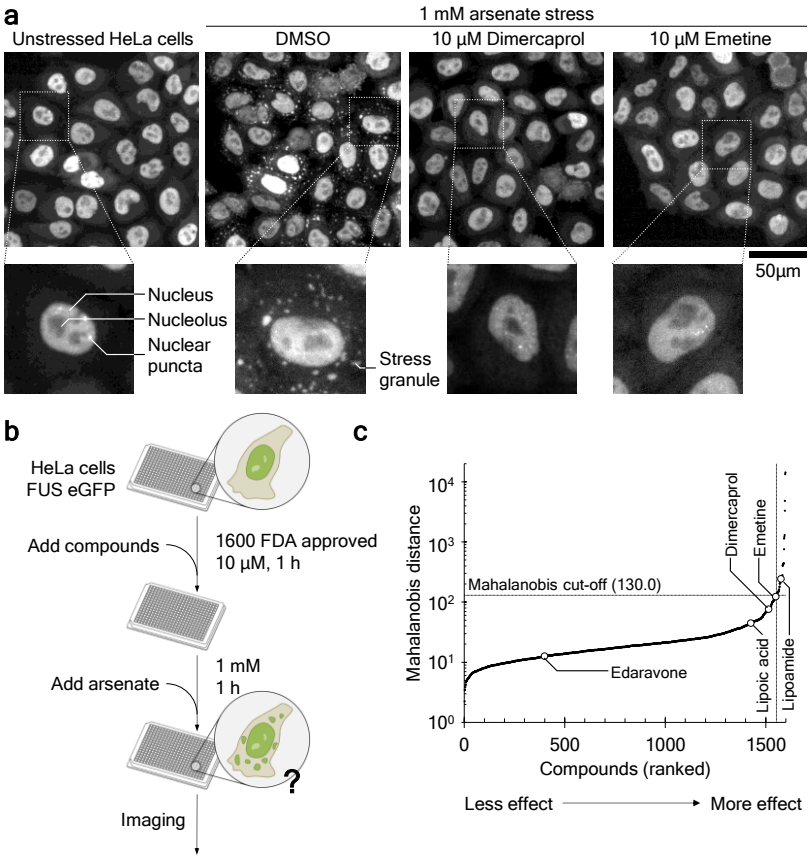

Figure 1. Screening for small compounds which affect stress granule formation *ex vivo* in HeLa cells. a) The sub-cellular localisation of FUS GFP in unstressed HeLa cells, stressed cells with compound solvent (DMSO) negative control, and with the positive controls dimercaprol and emetine. Stress causes nuclear export of FUS and formation of stress granules (cytoplasmic liquid FUS-containing condensates). **b)** Workflow for screening small molecules for effects on FUS GFP localisation in HeLa cells *ex vivo*. **c)** Ranked Mahalanobis distances for all 1600 compounds screened (mean from six fields of view) where high values indicate more compound effect. Several automated measures of FUS localisation were combined into a single Mahalanobis distance score; the largest contributor were cytoplasmic FUS condensate number and area. A cut-off of 130 was used to select 47 compounds for further analysis.

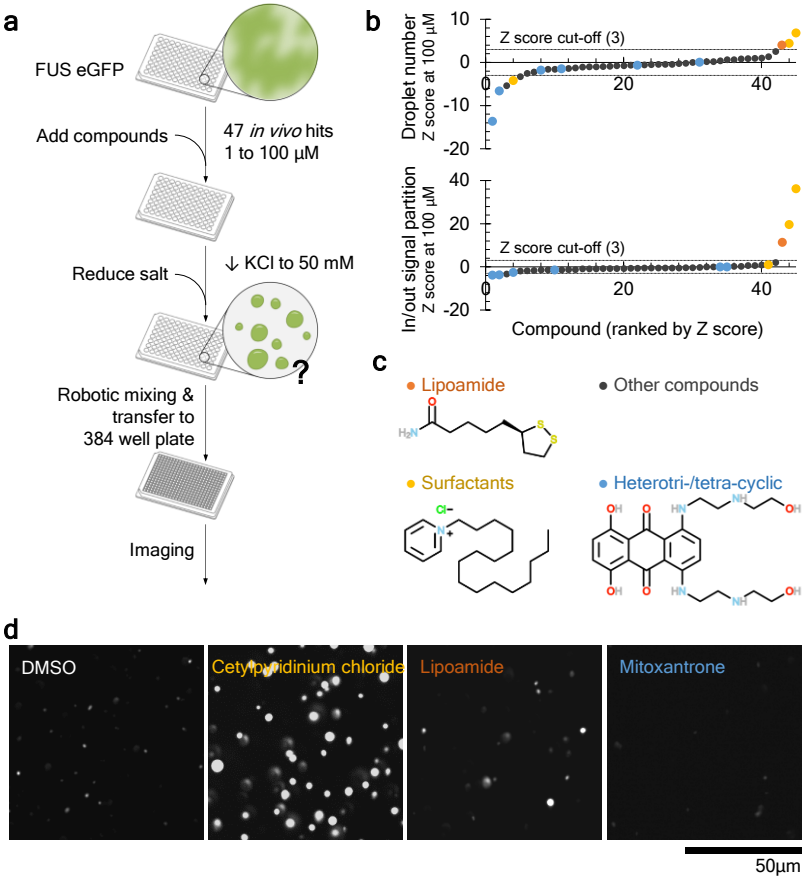

Figure 2. Screening for small compounds which affect FUS biomolecular condensate formation *in vitro.* **a)** Workflow for screening small molecules for effects on FUS liquid-liquid phase separation of purified FUS GFP *in vitro*. **b)** Ranked Z scores of change in condensate droplet number and signal partition into FUS GFP droplets (formed under low salt conditions) where larger positive or negative values mean more compound effect. Scores were calculated at the maximum concentration at which the compound solvent (DMSO) negative control had no significant effect; 100 µM. Lipoamide, surfactant and heterotri-/tetracyclic compounds are indicated by data point colour, see f). **c)** Examples of the three classes of hit; lipoamide, cetylpyridinium chloride (surfactants), mitoxantronte (heterotri-/tetracyclic compounds). **d)** Appearance of the droplets with compound solvent (DMSO) negative control or examples of compound classes: cetylpyridinium chloride (surfactant), lipoamide or mitoxantrone (heterotricyclic). Note the larger drops with cetylpyridinium chloride and lipoamide and the fewer smaller drops with mitoxantrone.

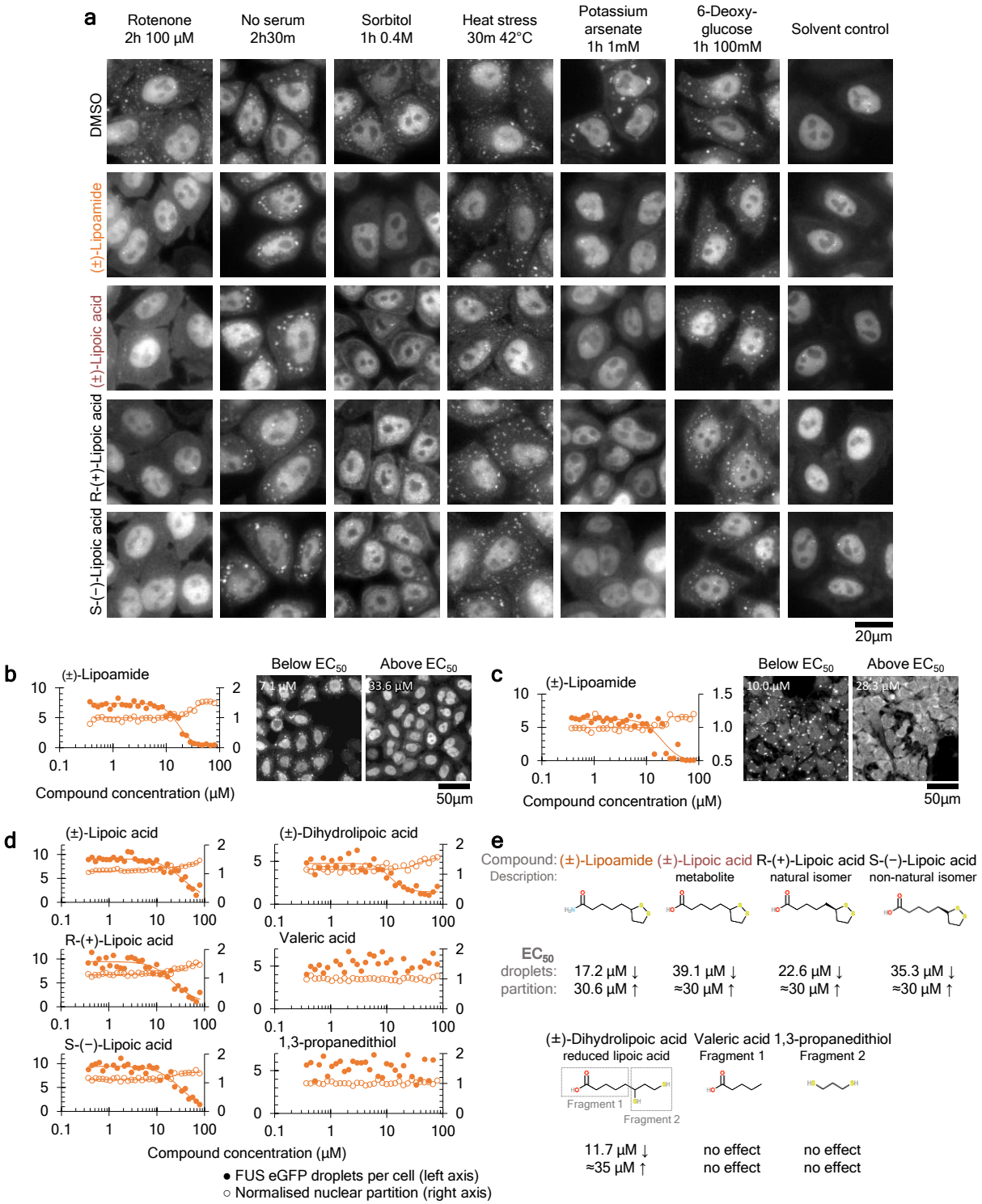

Figure 3. Activity of lipoamide-related compounds and action on different stresses constrains likely mechanisms of action. a) Images of HeLa cells expressing FUS GFP subject to different stresses – rotenone (mitochondrial), no serum, sorbitol (osmotic), heat, arsenate or 6-deoxyglucose (glycolysis) – with concurrent treatment with 10 µM lipoamide or isomers of lipoic acid. Lipoamide and lipoic acid are active against several stresses, including mitochondrial, osmotic and oxidative. **b)** Dose response of HeLa cell FUS GFP condensate number (●, left axis) and nuclear/cytoplasmic signal ratio (○, right axis) after 1h pre-treatment with lipoamide followed by 1 h arsenate stress with continued lipoamide treatment. **c)** Dose response of iPS cell FUS GFP condensate number and nuclear/cytoplasm ratio, as in b). **d)** Dose response of HeLa cell FUS GFP condensate number and

nuclear/cytoplasm ratio, with the same stress/treatment regime as b), for a range of compounds related to lipoamide. **e)** Summary of compounds structures and effect on cytoplasmic FUS condensate number and FUS nuclear partition.

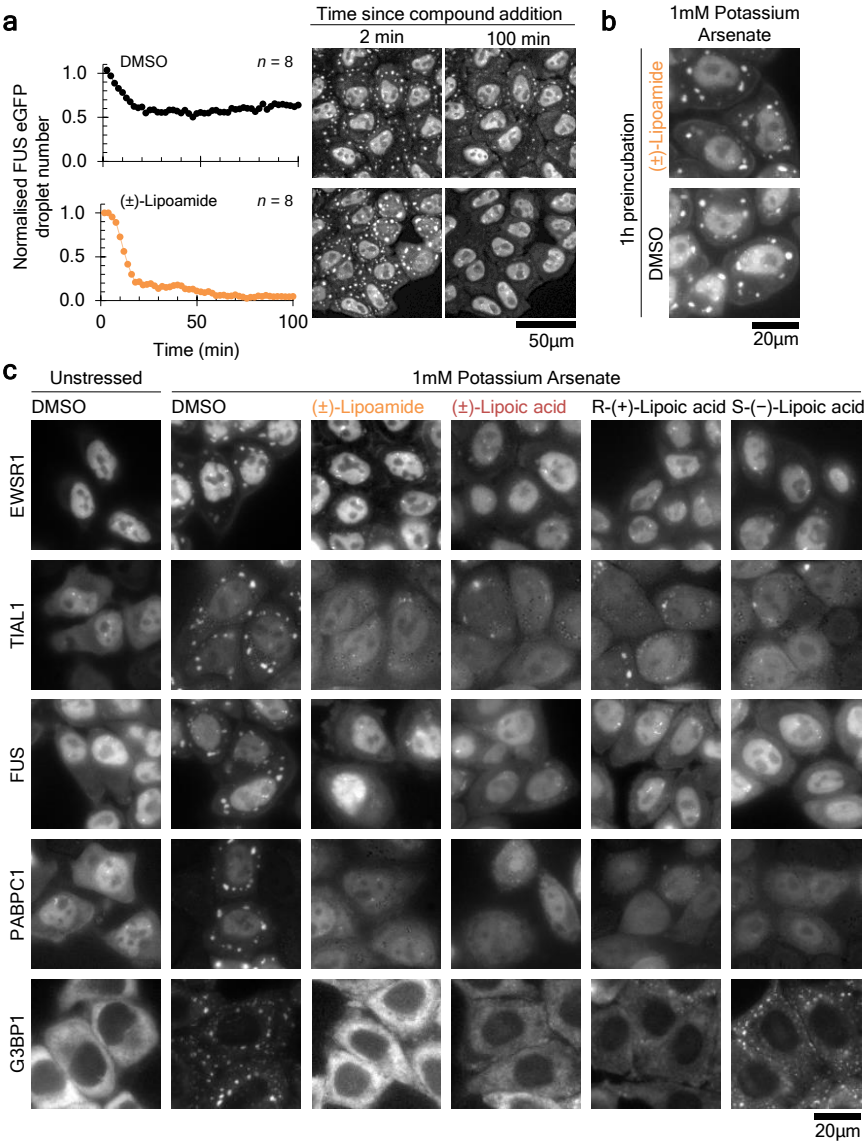

Figure 4. Lipoamide and lipoic acid prevent many proteins from entering stress granules under different stress regimes. a) Kinetics of loss of cytoplasmic FUS GFP condensates in HeLa cells pre-stressed for 1 h with arsenate then treated with 10 µM lipoamide (or DMSO solvent control) with continued arsenate stress. Example images 2 min and 100 min after addition of compound are shown on the right. Lipoamide can reverse the effect of existing arsenate stress. **b)** Images of HeLa cells expressing FUS GFP pre-treated with 10 µM lipoamide (or DMSO control) for 1 h, followed by 3 washes then 1 h arsenate stress. Lipoamide pre-treatment does not have a lasting effect on cells which prevents response to arsenate stress. **c)** Images of HeLa cells expressing GFP-labelled stress granule markers (EWSR1, TIAL1, PABC1 or G3BP1) following 1 h with arsenate stress and 10 µM lipoamide or isomers of lipoic acid, arsenate stress with DMSO solvent control, or DMSO without arsenate. Lipoamide and lipoic affect many stress granule components.

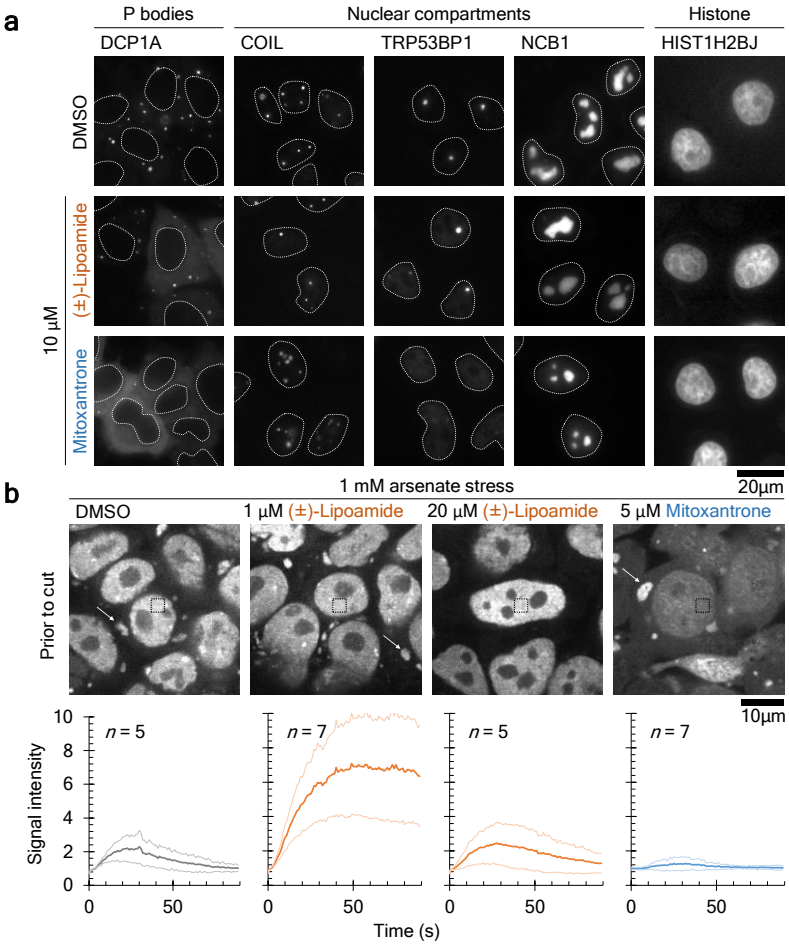

Figure 5. Lipoamide does not dissolve nuclear FUS compartments and other nuclear compartments. a) Images of HeLa cells expressing Protein GFP markers of other membraneless compartments subject to 1 h treatment with 10 µM compound (or DMSO control). Where unclear, the position of nuclei is indicated with a dotted outline. Lipoamide does not disrupt P bodies (DCP1A), Cajal bodies (COIL), DNA damage foci (TRP53BP1) or the nucleolus (NCB1), while mitoxantrone does have non-stress granule specific effects. **b)** Recruitment of FUS GFP to sites of UV laser-induced DNA damage in iPS cells after 1 h treatment with compound followed by 1 h arsenate stress. Top row shows FUS GFP fluorescence prior to the laser cut, stress granules are indicated with an arrow. Bottom row shows mean FUS GFP signal intensity response to DNA damage and one standard deviation above and below the mean. Mitoxantrone prevents formation of nuclear FUS condensates at the sites of DNA damage at under the cytoplasmic condensate number EC_{50} while lipoamide does prevent formation of nuclear FUS condensates.

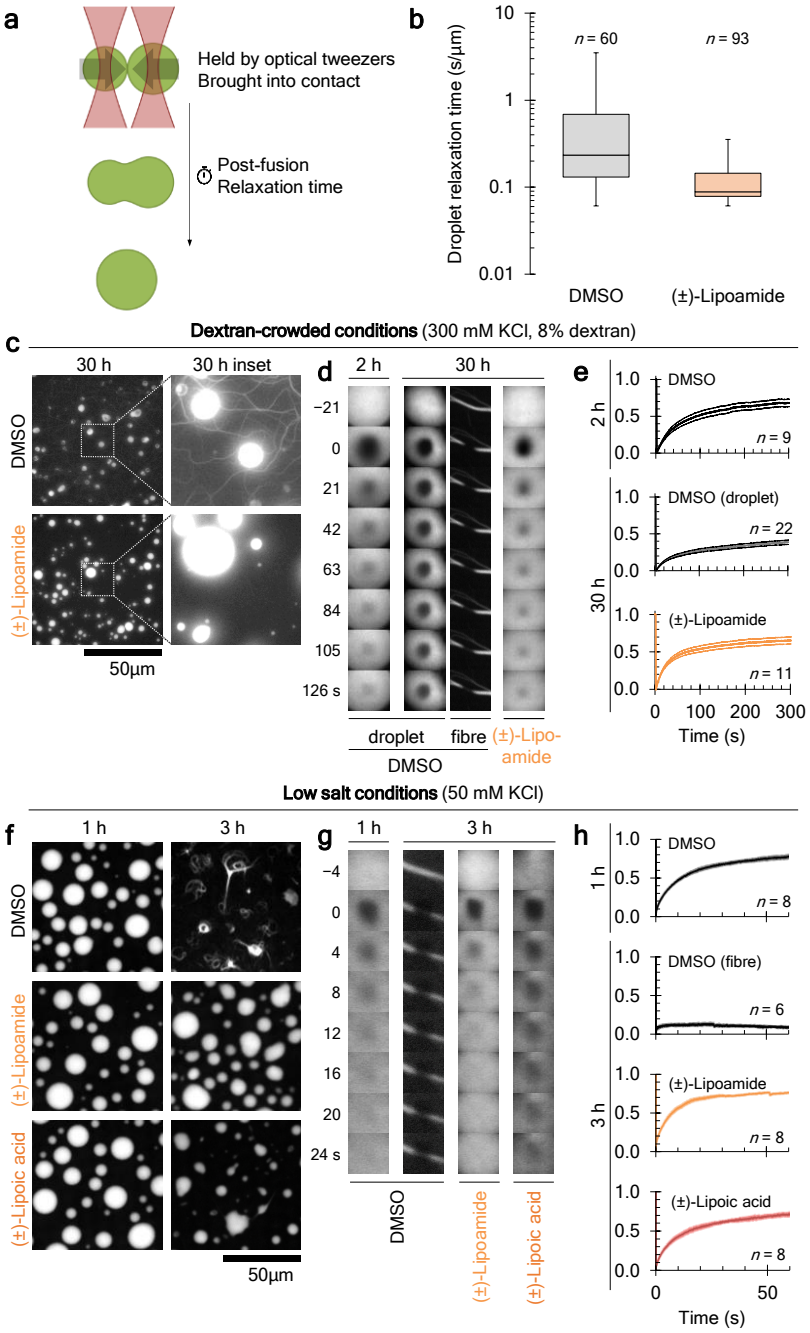

Figure 6. Lipoamide and lipoic acid affect FUS condensate properties and ALS-associated mutant FUS solidification *in vitro*. a) Schematic illustrating the quantitation of condensate droplet liquidity using optical tweezers. Two droplets are brought into contact and begin to fuse the time taken to relax to a single spherical droplet (once adjusted for droplet size) is a measure of the viscosity to surface tension ratio of the droplet – a measure of liquidity. Representative of two independent replicates. **b)** Droplet size-corrected relaxation times for droplet fusions with either 300 µM lipoamide or equivalent DMSO solvent control (0.3%). Box represents the 25th, 50th and 75th percentiles, whiskers represent 5th and 95th percentiles. Lipoamide reduces fusion time indicating lower viscosity and/or greater surface tension. **c-e)** Effect of 10 µM lipoamide on G156E FUS GFP condensates (formed under dextran crowding) on 'aging' while shaking, relative to an equivalent DMSO solvent control (0.1%). These conditions match those previously published[7]. **c)** Representative images after 30 h aging, showing fibre formation in the DMSO sample. **d)** Representative fluorescence recovery after photobleaching (FRAP) time series of FUS condensates and fibres during

aging. **e)** Quantitation of FRAP in c). Error bars represent starndard deviation. Aged condensates treated with lipoamide maintain large FUS GFP mobile fraction and short FRAP half-life while untreated condensates harden Effect of lipoamide and lipoic acid on G156E FUS GFP condensate 'aging' while shaking, relative to an equivalent DMSO solvent control (0.3%). Both compounds delay fibre formation. **f-h)** As for d-e), except using condensates formed under low salt conditions (more physiologically relevant) treated with 30 µM lipoamide or lipoic acid or an equivalent DMSO solvent control (0.3%).

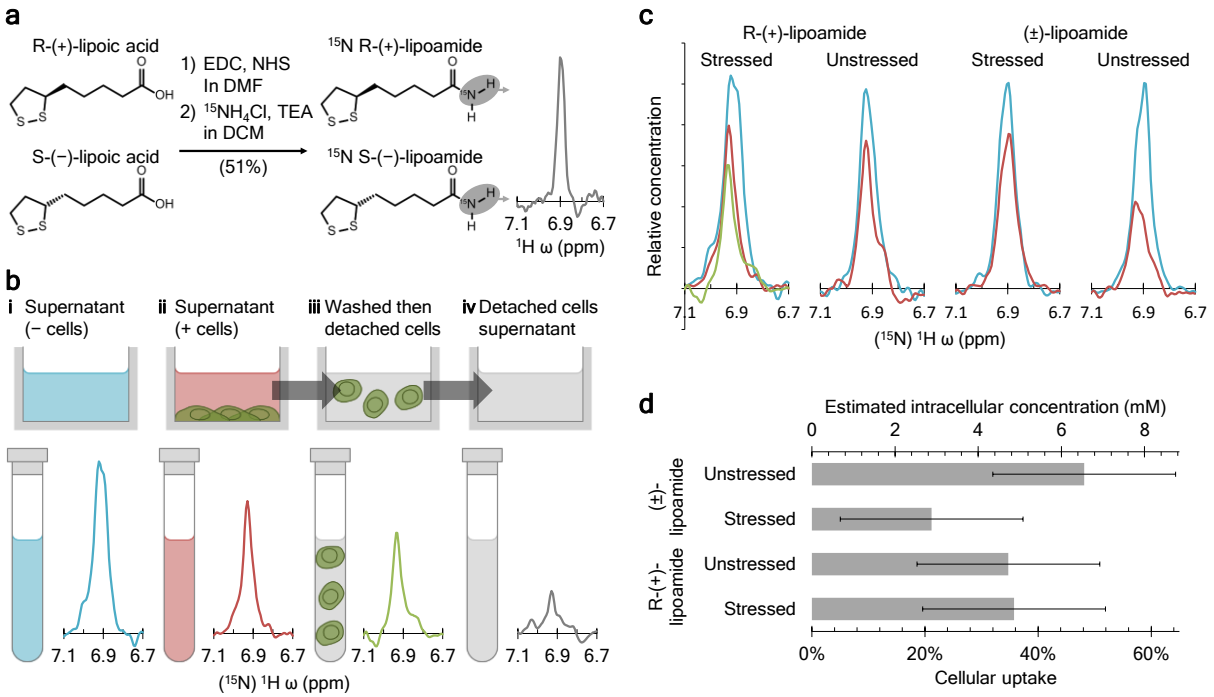

Figure 7. Lipoamide accumulates to high concentrations in cells without being metabolised. a) ^{15}N R-(+) and (±)-lipoamide were synthesised and characterised. Using a ^{15}N-edited ^{1}H-detected 1D HSQC NMR experiment, the two amide protons could be selectively detected in biological media and in HeLa cell pellets. The trans-amide proton (resonance at 6.9ppm) was amenable to quantification by NMR. Below pH 8.6, 10°C, the intensity of the signal was proportional to lipoamide concentration. For detail, see supplemental methods. **b)** Uptake of lipoamide by HeLa cells was measured by exposing cells to ^{15}N lipoamide then fractionating the samples and using NMR signal intensity from the trans-amide proton to measure ^{15}N lipoamide concentration. Medium with 100 µM ^{15}N lipoamide was incubated for 1 h in the absence or presence of HeLa cells. Following removal of medium, the cells were washed with medium (without arsenate) and detached using EDTA-trypsin. Solution or cell pellet/in-cell NMR was used to determine ^{15}N lipoamide concentration. Example spectra for cells stressed with 3 mM arsenate and incubated with R-(+)-lipoamide are shown with the same y axis scale. **c)** Cellular uptake was determined by subtracting signal from medium incubated with cells (red) from signal from medium without cells (cyan). This was carried out for all four combinations of stressed (3 mM arsenate) or unstressed cells with ^{15}N R-(+) or (±)-lipoamide. For stressed cells treated with ^{15}N R-(+)-lipoamide the high signal intensity from the washed cell sample (green) is consistent with the large uptake from the medium calculated from the with (red) and without cell (cyan) signal intensity. **d)** Quantitation of c) showing percentage uptake and calculated intracellular concentration, assuming that lipoamide is uniformly distributed within cells (see Supplemental Methods). Uncertainty in measurement was approximately 30% and there was no significant difference in uptake between conditions. All measurements indicated substantial uptake of lipoamide and cellular concentrations >1 mM.

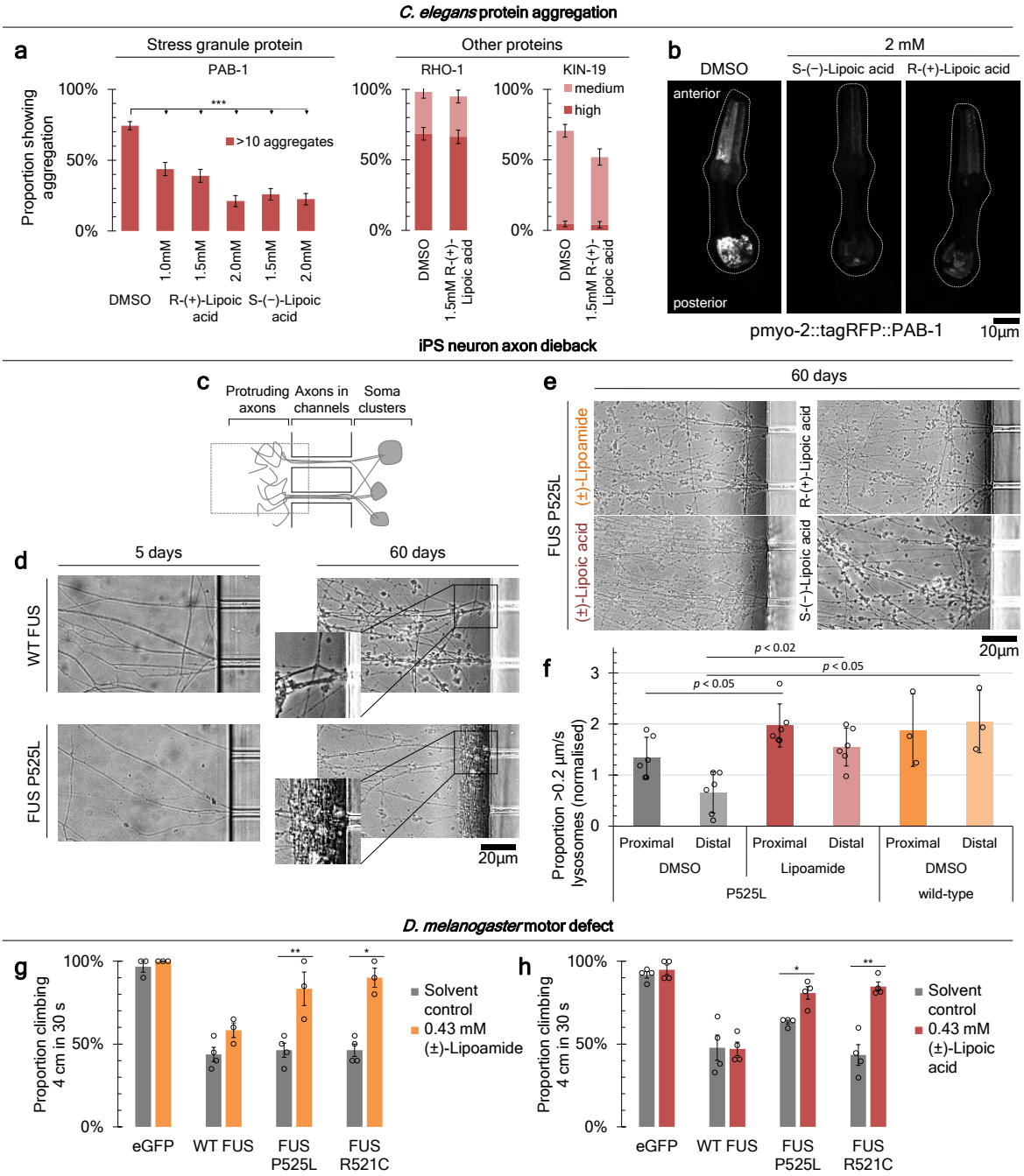

Figure 8. Lipoamide and lipoic acid have beneficial effects on *in vitro* and *in vivo* ALS models. a,b) Lipoic acid reduces age-induced aggregation of stress granule but not non-stress granule proteins in *C. elegans.* **a)** Toxicity and the effect on protein aggregation of R-(+) or S-(−)-lipoic acid in worms overexpressing fluorescently tagged proteins prone to aggregation. Incidence of PAB-1 aggregation in the pharyngeal muscles was scored from the proportion of cells with >10 aggregates. Incidence of RHO-1 and KIN-19 were scored on a low, medium, high scale – see methods. Both isomers of lipoic acid caused strong dose-dependent reduction of aggregation of PAB-1 but not RHO-1 or KIN-19. Significant changes from the DMSO control are indicated. *** p<0.0001, Fisher's exact test. Error bars represent standard error of proportion, n>100 for each sample. **b)** Z projections of confocal microscope stacks through the pharynx of worms expressing fluorescently tagged PAB-1 with or without lipoic acid treatment showing reduced aggregate number. **c-e)** Lipoic acid and lipoamide on dieback of neurons derived from iPS cells expressing FUS P525L, associated with familial ALS. **c)** Schematic of neuron culture, showing the channels through which the axons grow from the soma on

the right. The region shown in micrographs in d,e) is indicated. **d)** iPS-derived neurons after 5 days and 60 days in culture with 0.02% DMSO. Neurons expressing wild-type FUS have stable axons, while neurons expressing FUS P525L have unstable axons which die-back leaving material around the exit point of axons from the channels. **e)** iPS-derived neurons expressing FUS P525L after 60 days in culture in the presence of 2 µM lipoamide or racemic, R-(+) or S-(−)-lipoic acid. Representative images from a blinded experiment which also included the DMSO (solvent control) treated neurons shown in c). **f)** Proportion of lysotracker-labelled lysosomes moving with an average speed greater than 2 µm/s following 3 days treatment with 2 µM lipoamide or equivalent DMSO concentration solvent control for motor neurons expressing either P525L or wild-type FUS. *n* = 5 (P525L) or *n* = 3 (wild-type) biological replicates, analysing 5 axon bundles per replicate. Lipoamide significantly increased lysosome transport (Student's T-test). **g)** Lipoic acid recovers defects in motor function of *D. menalogaster* overexpressing human wild type FUS or ALS-associated FUS mutations. Overexpression of FUS leads to motor defects and the animals are unable to climb. Treatment with lipoic acid showed a dose-dependent increase in the ability of animals expressing wild-type FUS, FUS P525L or FUS R512C to climb. ** $p<0.005$, * $p<0.05$, one-way ANOVA. **h)** Lipoamide also recovers defects in motor function of *D. menalogaster.* Equivalent conditions to f) are shown, with lipoamide treatment in place of lipoic acid. * $p<0.05$, ** $p<0.005$, Student's T test.

Supplementary Figures

Supplementary Information

Synthesis and characterisation of Racemic (±) and ^{15}N R-(+)-lipoamide

^{15}N (±)-Lipoamide

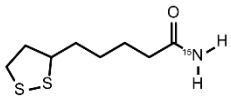

(±)-Lipoic acid (1.08 g, 5.24 mmol), N-Hydroxysuccinimide (660 mg, 5.60 mmol) and (1-ethyl-3-(3-dimethylaminopropyl) carbodiimide hydrochloride (1.1 g, 5.76 mmol) were stirred in DMF (20 ml) at 25 °C under argon atmosphere for 4 h. The solution was diluted with EtOAc (100 ml) and washed with H_2O (100 ml) and saturated aqueous $NaHCO_3$ (100 ml). The organic layer was dried over $MgSO_4$, filtered off and concentrated under reduced pressure. The NHS ester obtained, trimethylamine (1.1 ml, 7.89 mmol) and $^{15}NH_4Cl$ (500 mg, 9.36 mmol) were dissolved in DCM (20 ml) and the mixture was stirred for 20 h. The solution was diluted with DCM (100 ml), washed with H_2O (100 ml), saturated aqueous $NaHCO_3$ (100 ml) and again with H_2O (100 ml, 2 times). The organic layer was dried over $MgSO_4$, filtered off and concentrated under reduced pressure to give crude ^{15}N Lipoamide, which was further purified by silica gel column chromatography (DCM:MeOH=30:1). The solvent was removed under reduced pressure and ^{15}N Lipoamide was obtained as yellow solid. Yield: 554.2mg (51%). ^{1}H NMR (400 MHz, Chloroform-*d*) δ 5.62 (d, *J* = 31.3 Hz, 1H, NH_{cis}), 5.37 (d, *J* = 31.0 Hz, 1H, NH_{trans}), 3.60 (ddt, 1H, SSC*H*), 3.26 – 3.06 (m, 2H, SSCH_2), 2.58 – 2.40 (m, 1H, SSCH2CH_{trans}), 2.26 (t, *J* = 7.5 Hz, 2H, CH_2CONH$_2$), 2.02 – 1.84 (m, 1H, SSCH$_2$CH_{cis}), 1.83 – 1.60 (m, 4H), 1.60 – 1.39 (m, 2H, CH_2CH$_2$CH$_2$CONH$_2$). ^{13}C NMR (101 MHz, Chloroform-*d*) δ 175.02 (d, *J* = 13.6 Hz, *C*ONH$_2$), 56.39, 40.26, 38.49, 35.61, 35.53, 28.84, 25.14. ESI-MS: m/z = 229.05 (M+Na)+. Electrospray (M+Na)+ ion detected. Data suggests ^{15}N label is at ~99%. IR: 3352 cm^{-1}, 3176 cm^{-1} (CO*N*H_2), 2937 cm^{-1},2898 cm^{-1}, 2865 cm^{-1},2783 cm^{-1} (*C-H*), 1746 cm^{-1}, 1650 cm^{-1}, 1629 cm^{-1}, 1464 cm^{-1}, 1413 cm^{-1}, 1367 cm^{-1}, 1342 cm^{-1}, 1321 cm^{-1}, 1292 cm^{-1}, 1281 cm^{-1}, 1252 cm^{-1}, 1226 cm^{-1}, 1203 cm^{-1}, 1144 cm^{-1}, 1125 cm^{-1}, 1078 cm^{-1}, 1034 cm^{-1}, 999 cm^{-1}, 950 cm^{-1}, 911 cm^{-1}, 868 cm^{-1}, 803 cm^{-1}, 734 cm^{-1}, 675 cm^{-1}, 629 cm^{-1} (*C=O*). Melting point: 130 °C, Rf=0.60 (DCM:MeOH=20:1).

^{15}N R-(+)-Lipoamide

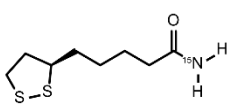

R-(+)-Lipoic acid (1.08 g, 5.24 mmol), N-Hydroxysuccinimide (660 mg, 5.60 mmol) and (1-ethyl-3-(3-dimethylaminopropyl)carbodiimide hydrochloride (1.1 g, 5.76 mmol) were stirred in DMF (20 ml) at 25 °C under argon atmosphere for 4 h. The solution was diluted with EtOAc (100 ml) and washed

with H_2O (100 ml) and saturated aqueous $NaHCO_3$ (100 ml). The organic layer was dried over $MgSO_4$, filtered off and concentrated under reduced pressure. The NHS ester obtained, trimethylamine (1.1 ml, 7.89 mmol) and $^{15}NH_4Cl$ (500 mg, 9.36 mmol) were dissolved in DCM (20 ml) and the mixture was stirred for 20 h. The solution was diluted with DCM (100 ml), washed with H_2O (100 ml), saturated aqueous $NaHCO_3$ (100 ml) and again with H_2O (100 ml, 2 times). The organic layer was dried over $MgSO_4$, filtered off and concentrated under reduced pressure to give crude ^{15}N Lipoamide, which was further purified by silica gel column chromatography (DCM:MeOH=30:1). The solvent was removed under reduced pressure and ^{15}N (*R*)-Lipoamide was obtained as yellow solid. Yield: 554.5mg (51%). ^1H NMR (400 MHz, Chloroform-*d*) δ 5.56 (d, *J* = 4.1 Hz, 1H, NH_{cis}), 5.34 (d, *J* = 4.7 Hz, 1H, NH_{trans}), 3.60 (ddt, 1H, SSC*H*), 3.30 – 3.03 (m, 2H, SSCH_2), 2.61 – 2.35 (m, 1H, SSCH2CH_{trans}), 2.32 – 2.18 (m, 2H, CH_2CONH$_2$), 1.94 (m, 1H, SSCH$_2$CH_{cis}), 1.81 – 1.59 (m, 4H), 1.59 – 1.41 (m, 2H, CH_2CH$_2$CH$_2$CONH$_2$). ^{13}C NMR (101 MHz, Chloroform-*d*) δ 174.90 (d), 56.40, 40.26, 38.50, 35.60, 35.52, 34.64, 28.85, 25.14. ESI-MS: m/z = 207.06 (M+H+). Electrospray (M+H+) ion detected. Data suggests ^{15}N label is at ~99%. IR: 3340cm^{-1}, 3174cm^{-1} (CO*N*H_2), 2936 cm^{-1},2921 cm^{-1}, 2865 cm^{-1},2850 cm^{-1} (*C-H*), 2788 cm^{-1}, 2550 cm^{-1}, 2360 cm^{-1}, 2341 cm^{-1}, 2161 cm^{-1}, 2036 cm^{-1}, 1751 cm^{-1}, 1650 cm^{-1}, 1627 cm^{-1} (*C=O*), 1461 cm^{-1}, 1411 cm^{-1}, 1369 cm^{-1}, 1343 cm^{-1}, 1317 cm^{-1}, 1294 cm^{-1}, 1260 cm^{-1}, 1213 cm^{-1}, 1197 cm^{-1}, 1135 cm^{-1}, 1036 cm^{-1}, 1004 cm^{-1}, 914 cm^{-1}, 878 cm^{-1}, 808 cm^{-1}, 794 cm^{-1}. Melting point: 121.5 °C, Rf=0.60 (DCM:MeOH=20:1), $[\alpha]_D^{25}$ +105.6 (*c*=2.0, $CHCl_3$).

Density functional theory (DFT) calculations were performed to confirm assignment of the lipoamide ^1H NMR spectrum. An optimised structure for lipoamide was generated using Gaussian098 from which shielding tensors were calculated, enabling isotropic and anisotropic components to be determined. DFT calculations used the B3LYP density functional with the 6-31G(d) basis set[81]. DFT calculations confirmed that the cis-amide proton 13 should have a larger chemical shift than the trans-amide proton 14 (Figure S3A), and that the proton bound to carbon 3 closest in proximity to the proton bound to carbon 2 should have a larger chemical shift than the other proton on carbon 3 (Figure S3A).

(^{15}N)^1H NMR of ^{15}N lipoamide

^1H detected ^{15}N edited ^1H sensitivity enhanced HSQC NMR (referred to here as (^{15}N)^1H) spectra were acquired on a narrow bore Varian solution state spectrometer operating with a fixed field strength of 14.1 T, equipped with a room-temperature probe. The free induction decay was recorded for an acquisition time of 0.0624 and a sweep with of 8 kHz recorded over 1000 and a recovery delays of 1 s. Typically, 10000 transients were collected giving a total experiment time of 3 h 1 min. The J coupling between the amide protons and the ^{15}N in H_2O samples was determined to be 96 Hz, and so

the transfer times of 1/4 J in the INEPT portions of the pulse sequence were set to 2.6 ms. With these settings ^{15}N ammonia or ammonium ions would not be detectable. Chemical modification of ^{15}N lipoamide (including covalent attachment to an apoenzyme) would give a substantial change in the (^{15}N)^{1}H NMR spectrum. Similarly, dissolution of lipoamide in a phospholipid membrane would give substantial peak broadening in the cell samples. We observed neither, consistent with freely diffusing lipoamide.

Integrated NMR signal intensity is proportional to concentration, provided conditions (including ionic strength, buffer composition, temperature and pH) are identical[82]. Chemical exchange[83], expected as the amide protons in lipoamide should be labile in water, must also be accounted for. To ensure appropriate conditions were selected, (^{15}N)^{1}H NMR spectra were obtained in different solvents (Chloroform-*d,* H_2O, culture medium, medium with 3 mM $KAsO_2$ and a 50:50 mixture of medium with 3 mM $KAsO_2$ and EDTA-trypsin) (Figure S3B,C). Only in pure water and Chloroform-*d* were both amide proton resonances of comparable signal intensity. In other solvents the cis-amide proton signal was reduced, suggesting chemical exchange (Figure S3B), therefore the trans-amide proton was used for concentration quantitation. To determine temperature and pH sensitivity of the trans-amide proton signal (^{15}N)^{1}H spectra of 1 mM lipoamide in medium were acquired at different temperatures (Figure S3D) and pH (Figure S3E). Both amide protons showed chemical exchange under high temperature, high pH conditions, with the trans-amide proton affected more weakly (Figure S3D,E). To determine whether lipoamide degrades over time the signal from the trans-amide proton was monitored at 37°C and 10°C for 10 h. At 37°C, but not 10°C, the signal intensity decayed slowly (Figure S3F), suggesting slow hydrolysis to form ammonia. At 10°C and below pH 8.6 the integrated signal from the trans-amide proton resonance is therefore a good measure of ^{15}N lipoamide concentration.

Cellular uptake was measured by comparing the signal intensity S of the trans-amide proton of lipoamide acquired in the absence ($-cells$, sample i, Figure 3B) and presence ($+cells$, sample ii, Figure 3B) of HeLa cells. The measured fractional uptake U was given by:

$$U = 1 - \frac{S_{+cells}}{S_{-cells}}$$

The quantity (moles) of lipoamide added (add) becomes distributed between the intracellular ($cell$) and extracellular (out) environments following uptake. This can be expressed in terms of concentrations c and volumes V:

$$c_{add}V_{add} = c_{cell}V_{cell} + c_{out}V_{out}$$

The total volume of cells is given by $V_{cell} = V_1 N_{cell}$ where V_1 is the volume of a single cell and N_{cell} is the number of cells. $V_{cell} \ll V_{add}$ so we assume $V_{add} = V_{out}$. The fractional uptake can also be written in terms of these concentrations and volumes:

$$U = 1 - \frac{c_{out} V_{out}}{c_{add} V_{add}}$$

Rearrangement gives expressions for the concentration inside and outside the cell in terms of the quantity of lipoamide added and the measured fractional uptake U.

$$C_{out} = (1 - U)\frac{c_{add} V_{add}}{V_{out}}$$

$$C_{cell} = U\frac{c_{add} V_{add}}{V_1 N_{cell}}$$

We approximate HeLa cells as spheres of radius 10^{-5} m $V_1 = 4.19 \times 10^{-15}$ m^3. In our experiment, $N_{cell} = 10^6$, $c_{add} = 100$ µM and $V_{add} = 600$ µl, respectively.

We saw no evidence for peak broadening which would be associated with dissolution in a phospholipid membrane, however in principle the lost signal intensity on uptake could be attributed to uptake into membranes rather than the cytoplasm. Calculation suggests this is implausible. The number of phospholipid molecules in the plasma membrane can be estimated from the footprint of each lipid molecule $A_L = 0.5$ nm^2 [84]. Assuming a spherical cell, the surface area of a single cell is $A_1 = 1.3 \times 10^{-9}$ m^2. Therefore, the total number of phospholipid on the cell surface is given by $N_L = \frac{A_1 N_{cell}}{A_L}$. The number of lipoamide molecules taken up by cells $N_{uptake} = c_{cell} V_{cell} N_A$ where N_A is Avogadro's number. The ratio R of lipoamide to lipid molecules is given by:

$$R = \frac{N_{uptake}}{N_L} = \frac{A_L N_A U c_{add} V_{add}}{A_1 N_{cell}}$$

For the mean experimentally observed $U = 0.35$ (ie. 35% uptake) then we expect $R = 4.9$, i.e. 4.9 lipoamide molecules per plasma membrane lipid molecule. The plasma membrane is not the only membrane in the cell, however even if it makes up 10% of total phospholipid there would need to be approximately 1 lipoamide molecule per 2 phospholipid molecules.

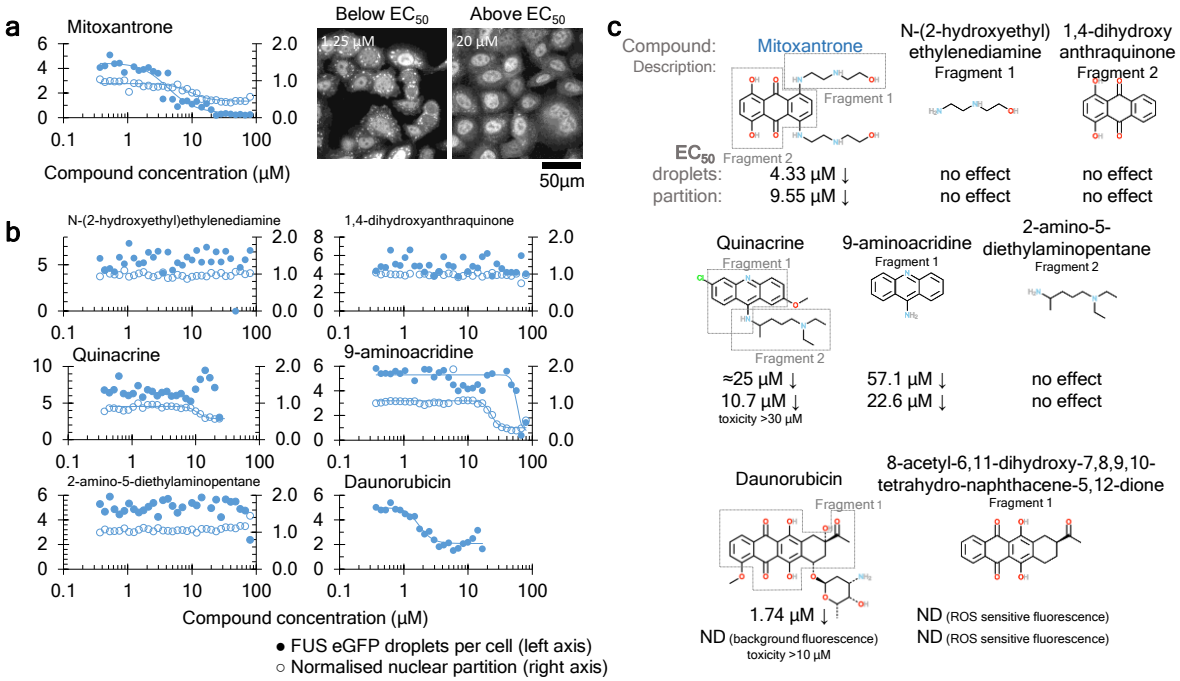

Figure S1. Structure activity relationship of heterotricyclic compounds implicates the tricyclic core as responsible for activity. a) Dose response of HeLa cell FUS GFP condensate number (●, left axis) and nuclear/cytoplasmic signal ratio (○, right axis) after 1h pre-treatment with mitoxantrone followed by 1 h arsenate stress with continued mitoxantrone treatment. **b)** Dose response of HeLa cell FUS GFP condensate number and nuclear/cytoplasm ratio, with the same stress/treatment regime as a), for a range of compounds related to mitoxantrone and other heterotricyclic hits, quinacrine and the tetracycline antibiotic family. **b)** Summary of compounds structures and effect on cytoplasmic FUS condensate number and FUS nuclear partition.

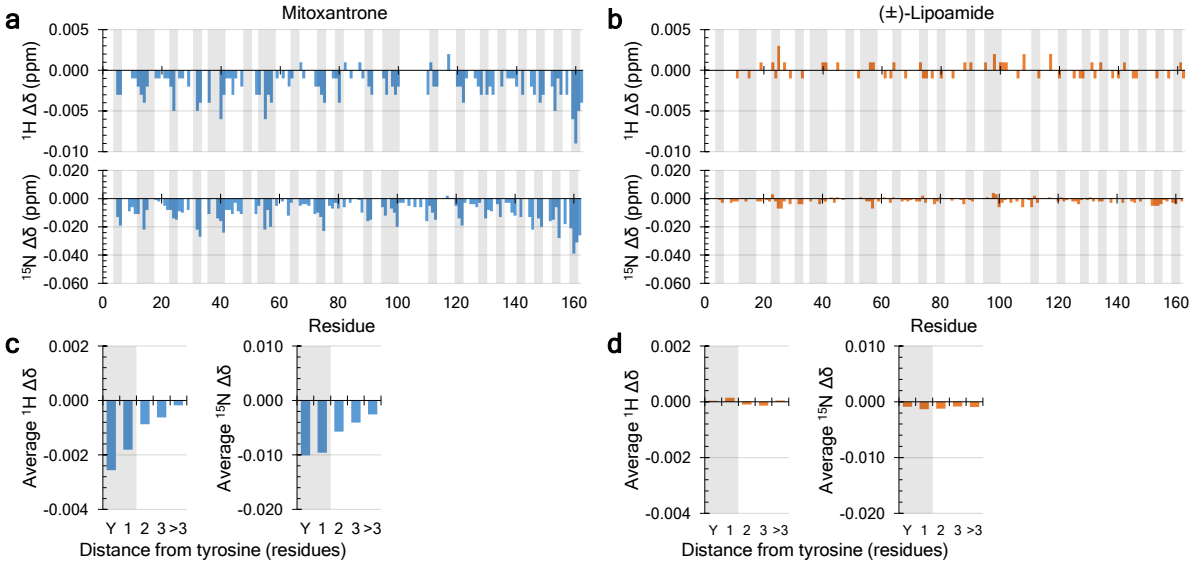

Figure S2. Lipoamide does not have NMR-detectable interaction with the low complexity PLD of FUS-like RBPs. a,b) NMR chemical shift deviations per residue for the FUS N-terminal PLD (residues 1 to 163) with **a)** 500 µM mitoxantrone or **b)** 500 µM lipoamide compared to the drug solvent control (1% DMSO). ^{1}H and ^{15}N shifts were observed for mitoxantrone across the entire PLD. Larger shifts tended to occur needed near tyrosine (Y) residues and light grey bars indicate tyrosine residues and residues neighbouring a tyrosine. **c,d)** Average ^{1}H and ^{15}N shifts across residues zero, one, two, three or more than three residues from a tyrosine in the presence of either mitoxantrone or lipoamide. In the presence of mitoxantrone, chemical shifts correlated with distance from tyrosine. No other residue showed a similar correlation.

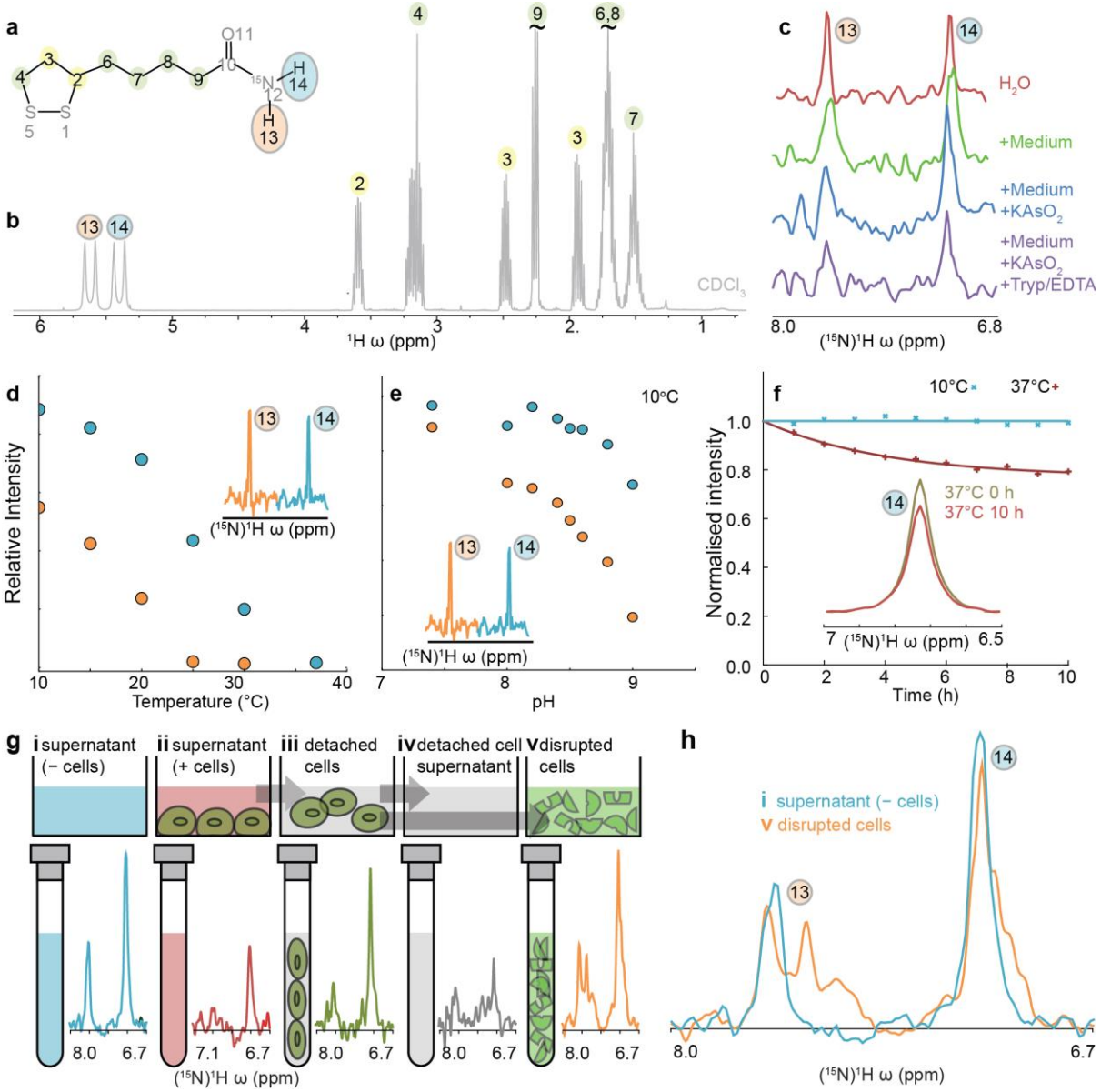

Figure S3. **Characterisation of ^{15}N Lipoamide by the ^{1}H NMR. a)** The chemical structure of ^{15}N lipoamide. **b)** Resonances in the ^{1}H NMR spectrum can be unambiguously assigned to individual protons of ^{15}N lipoamide in $CDCl_3$. **c)** ^{15}N filtered NMR experiments were acquired that show the cis-amide and trans-amide protons (environments 13 and 14 respectively) of lipoamide. The relative signal intensities sensitive to local solution conditions, indicating chemical exchange at 37°C. **d)** At pH 8.3, the intensity of both resonances decreased with increasing temperature. This indicated chemical exchange where local molecular dynamics and/or interactions with H_2O on ms to µs timescale reduce the signal. Below 15°C, the intensity of the trans-amide resonance (14) approaches a plateau, indicating a slow exchange regime where signal intensity is an unambiguous measure of concentration. **e)** At 10°C, the intensity of the cis- and trans-amide proton resonances increased with decreasing pH indicating the presence of ms to µs second dynamics. Below pH 8.6, the intensity of the trans-amide proton was constant, indicating a slow exchange regime. Together, d) and f) indicate at 10°C and below pH 8.6 integrated signal intensity of the trans-amide proton of lipoamide in ^{15}N edited ^{1}H NMR experiments is a reliable proxy for concentration. **f)** Signal intensity of the trans-amide proton of lipoamide, when dissolved in growth medium, decreased over time at 37°C but not at 10°C. At 10°C signal intensity is stable for >10 h experiments. **g)** The signal intensity of both the cis- and trans- amide protons under different experimental conditions. This is an expanded version

of Figure 7B, which only shows the trans-amide proton, and includes one additional condition: v) Cells (from iii) disrupted with Triton X-100 and DNaseI. Taken together, i) to iv) imply lipoamide is taken up by HeLa cells in a mobile form while most of the molecules were unmodified (with uptake quantified in Figure 7C-D). **h)** An expanded view of the spectra in g) i) and v). On disruption of cells with Triton X-100 and DNaseI the spectrum changed significantly, indicating chemical modification of lipoamide when cellular compartments are disrupted.

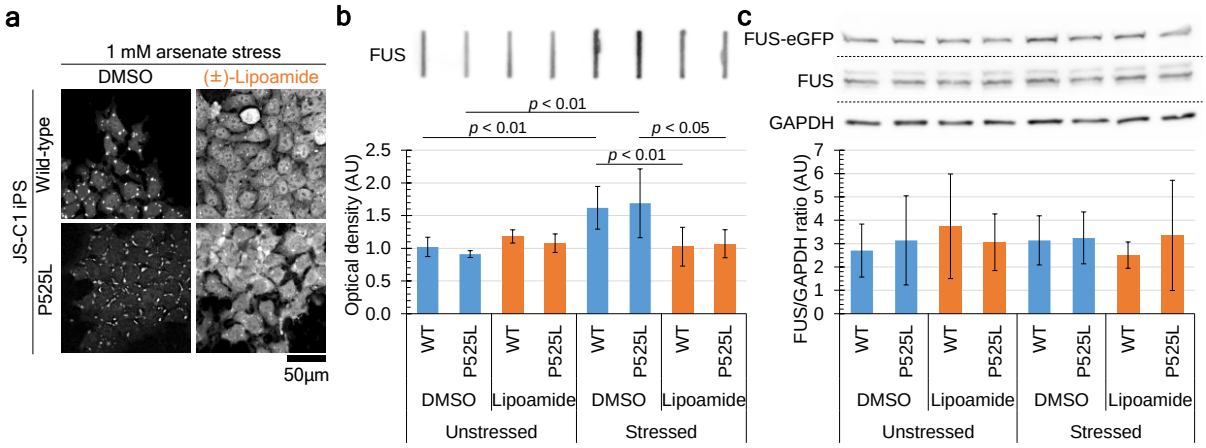

Figure S4. Lipoamide reduces wild-type and P525L FUS intracellular aggregates in iPS cells. a) FUS GFP localisation in isogenic iPS cells expressing either wild-type or P525L FUS GFP under combinations of 1h arsenate stress followed by 1 h stress with 30 µM lipoamide or DMSO negative control treatment. FUS P525L causes formation of larger cytoplasmic FUS condensates which are still sensitive to lipoamide. **b)** Relative optical densities of aggregated FUS assessed by filter retardation from the iPS cells in a) following 1 h pre-treatment with 100 µM lipoamide or DMSO solvent control followed by 1 h arsenate stress or no stress. Significant changes (Student's t-test) are indicated, *n* = 5. **c)** Anti-FUS and anti-GAPDH Western blots following the cell treatments in b). No significant change in FUS expression level relative to GAPDH was detected (Student's t-test, *n* = 3).